REPORT DOCUMENTATION PAGE

Form Approved OMB NO. 0704-0188

1. REPORT DATE (DD-MM-YYYY)	2. REPORT TYPE	3. DATES COVERED (From - To)
12-02-2018	Final Report	17-Jan-2017 - 31-Dec-2017

4. TITLE AND SUBTITLE
Final Report: Mesh-sequenced Realizations for Evaluation of Subgrid-Scale Models for Turbulent Combustion (Short Term Innovative Research program)

5a. CONTRACT NUMBER
W911NF-17-1-0074

5b. GRANT NUMBER

5c. PROGRAM ELEMENT NUMBER
611102

6. AUTHORS

5d. PROJECT NUMBER

5e. TASK NUMBER

5f. WORK UNIT NUMBER

7. PERFORMING ORGANIZATION NAMES AND ADDRESSES
North Carolina State University
2701 Sullivan Drive
Admin Srvcs III, Box 7514
Raleigh, NC 27695 -7514

8. PERFORMING ORGANIZATION REPORT NUMBER

9. SPONSORING/MONITORING AGENCY NAME(S) AND ADDRESS (ES)
U.S. Army Research Office
P.O. Box 12211
Research Triangle Park, NC 27709-2211

10. SPONSOR/MONITOR'S ACRONYM(S)
ARO

11. SPONSOR/MONITOR'S REPORT NUMBER(S)
70391-EG-II.3

12. DISTRIBUTION AVAILIBILITY STATEMENT
Approved for public release; distribution is unlimited.

13. SUPPLEMENTARY NOTES
The views, opinions and/or findings contained in this report are those of the author(s) and should not contrued as an official Department of the Army position, policy or decision, unless so designated by other documentation.

14. ABSTRACT

15. SUBJECT TERMS

16. SECURITY CLASSIFICATION OF:			17. LIMITATION OF ABSTRACT	15. NUMBER OF PAGES	19a. NAME OF RESPONSIBLE PERSON
a. REPORT	b. ABSTRACT	c. THIS PAGE			Jack Edwards
UU	UU	UU	UU		19b. TELEPHONE NUMBER 919-515-5264

RPPR Final Report
as of 15-Feb-2018

Agency Code:

Proposal Number: 70391EGII **Agreement Number: W911NF-17-1-0074**
INVESTIGATOR(S):

Name: Jack Edwards
Email: jredward@ncsu.edu
Phone Number: 9195155264
Principal: Y

Organization: **North Carolina State University**
Address: 2701 Sullivan Drive, Raleigh, NC 276957514
Country: USA
DUNS Number: 042092122 EIN: 566000756

Report Date: 31-Mar-2018 Date Received: 12-Feb-2018
Final Report for Period Beginning 17-Jan-2017 and Ending 31-Dec-2017
Title: Mesh-sequenced Realizations for Evaluation of Subgrid-Scale Models for Turbulent Combustion (Short Term Innovative Research program)
Begin Performance Period: 17-Jan-2017 **End Performance Period:** 31-Dec-2017
Report Term: 0-Other

Submitted By: Jack Edwards Email: jredward@ncsu.edu
Phone: (919) 515-5264

Distribution Statement: 1-Approved for public release; distribution is unlimited.

STEM Degrees: 0 **STEM Participants:** 1

Major Goals: This work develops a new analysis approach, termed 'Multi-Resolution Analysis through Mesh-Sequenced Realizations (MRA-MSR)', for the evaluation of subgrid-scale (SGS) effects on apparent reactivity as expressed at a given mesh level. Attention is focused on the general problem of large-eddy simulation of turbulent combustion using finite-rate chemistry, which requires a direct integration of a (large) number of species conservation equations. The closure problem hinges on the evaluation of the filtered chemical production rates. In MRA/MSR, simultaneous large-eddy simulations of a reactive flow are performed at different mesh resolution levels. The solutions at each coarser mesh level are constrained by the filtered fine-mesh velocity, thus ensuring a strong correlation of eddy structures. The availability of data at each mesh level enables a detailed assessment of the effects of unresolved fluctuations on instantaneous and averaged predictions as well as the discovery of scaling relationships that might enable the construction of new subgrid models.

Accomplishments: 1. A new three-level MRA-MSR method was developed and tested. This approach conducts simultaneous, constrained large-eddy simulations at three different mesh levels as a means of connecting reactive scalar information at different scales of resolution. Constraining by the fine-mesh velocity field is employed to ensure correlation of eddy structures; other methods of constraining include the replacement of chemical production rates with those filtered from the underlying fine mesh and the construction of 'exact' forms for subgrid mass, momentum, and energy transport based on the underlying fine-mesh data.

2. The approach was tested for a bluff-body stabilized, non-premixed methane / hydrogen flame experimentally mapped at the University of Sydney. Meshes ranging from ~1.6 M cells to 108 M cells were employed. A seven-mesh MRA-MSR hierarchy was used, with the fine 'parent' mesh provided data to constrain three 'medium' meshes and three 'coarse' meshes. Independent (unconstrained) realizations were performed at different mesh levels to assess predictive capability. . Comparisons with experimental scalar and velocity data show generally good agreement with measured trends, with the most noteworthy deficiencies being an inaccurate prediction of the maximum fuel jet penetration distance and a reduced rate of CO to CO2 conversion near the face of the bluff body. The predictions at all mesh levels are sensitive to the imposed outer boundary condition, with a reflective slip-surface boundary condition resulting in higher levels of fluctuation intensity in the recirculation region. The use of a minimally-reflective boundary condition reduces the turbulence intensity, leading to a more elongated recirculation zone. The structure of the actual flame seems to be bracketed by these values

3. The MRA-MSR database was then used to analyze reactive-scalar behavior at different mesh levels. Several interesting trends emerged.

a. the use of 'source' and 'transport' coupling was found to be ineffective, leading to errors in minor-species predictions. Velocity coupling alone should be used in further MRA-MSR studies.

b. Scatterplot correlations of chemical production terms filtered from the underlying fine mesh with those calculated using evolved coarse-mesh data show a clear trend of diminishing apparent reactivity due to unresolved fluctuations at high subgrid Damköhler numbers.

c. Single-point, single-time filtered density functions of a locally normalized subgrid Damköhler number (a measure of the distribution of inverse chemical time scales in the neighborhood of a particular spatial location) show a characteristic beta-PDF form and display a large degree of scale similarity. This new observation could impact the design of turbulence / chemistry interaction models, but it is unclear whether it is restricted to non-premixed flames.

d. A priori analysis of NCSU's Least-Squares Minimization (LSM) turbulence / chemistry subgrid closure using MRA-MSR data shows that this model can capture the observed diminishment in apparent reactivity at high subgrid Damköhler numbers but cannot reduce the scatter significantly.

e. A new LSM variant based on the aforementioned observation of a characteristic beta-PDF form for the normalized subgrid Damköhler number has been developed and tested. This shows the potential of MRA-MSR in guiding new model developments.

A major goal of the MRA-MSR framework is to discover influences of unresolved information on apparent reactivity as expressed at a particular mesh level and to use this information to construct improved closure models. This goal has been partially realized from the activities undertaken under the STIR grant. More details can be found in the attached report.

Training Opportunities: The STIR grant partially supported one student, Tanner Nielsen, who is working toward his Ph.D. Tanner's activities in this scope included mesh-generation for the Sydney burner, the development of time-dependent, general, characteristic boundary conditions used in the simulations, and the development of some of the data-mining tools used in this investigation.

Results Dissemination: The results of this effort were presented at the AIAA 2018 SciTech meeting (Jan. '18) and at the AFOSR / ARO grantees meeting (June '17). A final briefing was presented to Dr. Anthenien at NCSU on Nov. 17, 2017. Some results from MRA-MSR were also presented at a seminar delivered by Dr. Edwards at Florida State University in August, 2017.

Honors and Awards: Nothing to Report

Protocol Activity Status:

Technology Transfer: Discussions of the potential of MRA-MSR in providing a means of assessing and developing new closure models were held with Dr. Tomasz Drozda and Dr. Robert Baurle of NASA Langley during the SciTech '2018 meeting. NASA is interested in ways of evaluating subgrid models for scramjet combustion.

PARTICIPANTS:

Participant Type: PD/PI
Participant: Jack Edwards
Person Months Worked: 1.00 **Funding Support:**
Project Contribution:
International Collaboration:
International Travel:
National Academy Member: N
Other Collaborators:

Participant Type: Graduate Student (research assistant)
Participant: Tanner Nielsen

RPPR Final Report
as of 15-Feb-2018

Person Months Worked: 9.00 **Funding Support:**
Project Contribution:
International Collaboration:
International Travel:
National Academy Member: N
Other Collaborators:

CONFERENCE PAPERS:

Publication Type: Conference Paper or Presentation **Publication Status:** 3-Accepted
Conference Name: AIAA SciTech 2018
Date Received: 29-Aug-2017 Conference Date: 08-Jan-2018 Date Published: 08-Jan-2018
Conference Location: Kissimmee, Florida
Paper Title: Mesh-Sequenced Realizations for Evaluation of Subgrid-Scale Models for Turbulent Combustion
Authors: Jack, Edwards
Acknowledged Federal Support: **Y**

Publication Type: Conference Paper or Presentation **Publication Status:** 1-Published
Conference Name: 2018 AIAA SciTech
Date Received: 09-Feb-2018 Conference Date: 08-Jan-2018 Date Published: 08-Jan-2018
Conference Location: Kissimmee, Florida
Paper Title: Mesh-Sequenced Realizations for Evaluation of Subgrid-Scale Models for Turbulent Combustion
Authors: Jack Edwards, Tanner Nielsen
Acknowledged Federal Support: **Y**

Mesh-Sequenced Realizations for Evaluation of Subgrid-Scale Models for Turbulent Combustion
W911NF-17-1-0074

Jack Edwards
Principal Investigator
Mechanical and Aerospace Engineering
North Carolina State University

Executive Summary

Recent sponsorship under ARO's STIR program has resulted in the development of a promising new technique for assessment, optimization, and improvement of subgrid-scale (SGS) models for turbulent combustion. The approach, termed Multi-Resolution Analysis through Mesh-Sequenced Realizations (MRA-MSR), conducts simultaneous, constrained large-eddy simulations on a set of hierarchically-coarsened meshes. The availability of underlying fine-mesh (subgrid) data corresponding to coarse-mesh locations allows a clearer assessment of the effects of unresolved fluctuations. The specific focus of MRA-MSR is the *formidable problem of the closure of the filtered chemical production terms* in large-eddy simulation, though the technique could be used to analyze any subgrid closure.

A key to MRA-MSR is the correlation of eddy structures at coarser mesh levels, which is facilitated by the transfer of filtered fine-mesh velocity information to the coarse meshes and its use in constraining the coarse-mesh velocity field. Initial applications of MRA-MSR have been focused on the Sydney bluff-body stabilized methane-hydrogen flame HM1E, which is a classical non-premixed flame with moderate strain effects in the 'necking' region. A three-level mesh sequence has been used, with the finest mesh containing ~105 M cells. A finite-rate methane oxidation mechanism, consisting of 17 reactive species plus inert nitrogen, has been employed. Major observations obtained from the STIR study are summarized as follows

1. Scatterplot correlations of chemical production terms filtered from the underlying fine mesh with those calculated using evolved coarse-mesh data show a clear trend of *diminishing apparent reactivity* due to unresolved fluctuations at high subgrid Damköhler numbers.

2. Single-point, single-time filtered density functions of a locally normalized subgrid Damköhler number (a measure of the distribution of inverse chemical time scales in the neighborhood of a particular spatial location) *show a characteristic beta-PDF form and display a large degree of scale similarity.* This new observation could impact the design of turbulence / chemistry interaction models, but it is unclear whether it is restricted to non-premixed flames.

3. *A priori* analysis of NCSU's Least-Squares Minimization (LSM) turbulence / chemistry subgrid closure using MRA-MSR data shows that this model can capture the observed diminishment in apparent reactivity at high subgrid Damköhler numbers but cannot reduce the scatter significantly.

4. A new LSM variant based on the aforementioned observation of a characteristic beta-PDF form for the normalized subgrid Damköhler number has been developed and tested. *This shows the potential of MRA-MSR in guiding new model developments.*

A major goal of the MRA-MSR framework is to discover influences of unresolved information on apparent reactivity as expressed at a particular mesh level and to use this information to construct improved closure

models. The potential of MRA-MSR in this scope has been demonstrated during the course of the STIR project, paving the way for future efforts that a.) refine the methodology further, b.) use it to develop additional multi-resolution databases suitable for interrogation, and c.) develop advanced analytical methods to assess and optimize existing model forms and to create new ones.

Project Development

The attached technical paper provides complete details of the work performed during the STIR project.

Project Challenges

This section discusses some of the challenges experienced during this project.

1. Need for low-speed flow solver capability. For the last 15 years or more, the Edwards group has worked mostly in high-speed turbulent combustion. In this realm, the boundary conditions are generally simpler, as the flows are usually confined and as the inflow / outflow conditions are usually supersonic. Furthermore, classical formulations for the discretization and integration of the compressible Navier-Stokes equations can be employed. For the lower-speed flows considered in this study, several major modifications to the Edwards group's software were incorporated, including

a.) development of a 'pressure based' implicit formulation that solved for the pressure directly, along with species mass fractions.

b.) addition of a previously-developed 'all-speed' flux formulation that reverts to a method consistent in the incompressible limit as the Mach number reduces toward zero. This approach had to be extended to multi-component, reactive mixtures for the purposes of this project.

c.) addition of time-dependent, locally one-dimensional, characteristic boundary conditions to provide a controllable level of reflectivity at inflow and outflow boundary conditions. As discussed in the paper, the solutions obtained were very sensitive to this choice.

d.) development of minimally-dissipative higher-order discretization methods suitable for low-Mach, reactive flows. In our high-speed code, a blend between a fourth-order central difference and PPM based on a divergence / vorticity switch is utilized; this approach was found to be ineffective at low speeds, and a hybrid version that uses fourth-order differencing only for the velocity field was developed. It must be stated that this approach was only partially effective; the results obtained still appear to be overly diffusive.

2. Need for a better synthetic eddy generation method. The best literature predictions of the Sydney flame use synthetic-eddy generation techniques to energize the co-flow. This accelerates the growth of resolvable eddies in the shear layer formed as the co-flow spills over the cylindrical bluff-body and also mimics the effects of free-stream turbulence, which may impact the mixing / reaction zone further downstream. Though we have a synthetic-eddy method at our disposal, it did not work well, yielding structures that were too small or too uncorrelated to result in significant acceleration of eddy growth. This deficiency led to a diminished level of predictive capability in some regions of the flame. Improvement of this aspect, along with further reductions in the level of numerical dissipation, are expected to provide significant benefits for future calculations.

Project Outcomes – More Recent Results

As described in the attached paper, MRA-MSR databases can be used to assess the potential of subgrid models for the filtered species production rates, as 'exact' expressions for these terms can be found simply by filtering the underlying fine-mesh solutions. The ratio of norms of the species production rates evaluated using a subgrid model to those calculated using exact data provides a measure of the efficacy of a model in replicating the influence of unresolved fluctuations. In this addendum to the report, we further discuss the use of MRA-MSR data to evaluate different variants of NCSU's Least Squares Minimization (LSM) closure. LSM, as mentioned in the paper, models the influences of unresolved fluctuations by a flow-dependent enhancement factor: $\overline{\dot{\omega}_s(q)} = f_{LSM}\,\dot{\omega}_s(\bar{q})$, where

$$f_{LSM} = \frac{\sum_s \overline{\dot{\omega}_s(q)}|_{\mathrm{mod}}\,\dot{\omega}_s(\bar{q}) + A^2\,|\sum_s h^f_{0,s}\,\overline{\dot{\omega}_s(q)|_{\mathrm{mod}}}\,\|\sum_s h^f_{0,s}\dot{\omega}_s(\bar{q})|}{\sum_s \dot{\omega}_s(\bar{q})\dot{\omega}_s(\bar{q}) + A^2(\sum_s h^f_{0,s}\dot{\omega}_s(\bar{q}))^2}$$

In the calculations described next, A in the above equation is set to zero. Different variants of LSM result from different choices of $\overline{\dot{\omega}_s(q)}|_{\mathrm{mod}}$. Given a neighborhood defined as the 27 cells that are neighbors of a particular mesh cell (including the cell itself), $\overline{\dot{\omega}_s(q)}|_{\mathrm{mod}}$ can be expressed as a linear combination of the species production rates:

$$\overline{\dot{\omega}_s(q)}|_{\mathrm{mod}} = \mathrm{sgn}(\dot{\omega}_s(\bar{q}))\,|\sum_k \alpha_k \dot{\omega}_s(\bar{q}_k)|$$

with the choice of weighting factors α_k being specific to the variant. For example, the weighting factors can be used to approximate an explicit filtering operation at the 1 Δ level or the 2 Δ level, essentially approximating a radial distribution function. As discussed in the paper, the use of a beta PDF distribution defined with respect to a normalized Damköhler number leads to another set of weighting factors. A least-squares solution to the minimization problem $f_{LSM-exact} = \min_f[\sum_s(\overline{\dot{\omega}_s(q)} - f\dot{\omega}_s(\bar{q}))^2]$ can be found if fine-mesh data is utilized. A similar, nearly optimal solution may be found by setting $\overline{\dot{\omega}_s(q)}|_{\mathrm{mod}}$ to be the neighborhood value *k* that minimizes

$$\min_k \sum_s (\overline{\dot{\omega}_s(q)} - \dot{\omega}_s(\bar{q}_k))^2$$

The exact least-squares solution is not realizable within an actual simulation, as it directly utilizes fine-mesh data that would not ordinarily be available. The 'nearly optimal' solution is a more realistic target point, however, as the actual value of the enhancement factor uses resolved-scale data – only the decision process uses the fine-mesh data.

Figure 1 compares the logarithm of norm ratios (filtered fine to modeled coarse) versus the logarithm of the coarse-mesh production-rate L2 norm for several LSM variants. The presentation is somewhat different than in the paper, serving to highlight scatter at moderate Damköhler numbers while de-emphasizing high and very low values. The degree of collapse about the zero line indicates the success of the model in capturing the filtered-fine mesh response. It is clear that even the exact least-squares model cannot precisely model all effects, particularly at lower Damköhler numbers. The 'nearly optimal' formulation performs less well but still narrows the distribution more than any of the other models shown (laminar chemistry (LC), 1 Δ explicit filtering, 2 Δ explicit filtering and β FDF). All models improve upon laminar chemistry by altering the slope of the distribution so that it becomes more horizontal; the 2 2 Δ explicit filtering and β FDF variants perform better than 1 Δ explicit filtering in altering the slope and

in reducing the scatter. The β FDF model performs slightly better than the 2 Δ explicit filtering model in terms of reducing scatter. The final word on the LSM family of models as analyzed using MRA-MSR is that they do not possess enough degrees of freedom to reduce scatter significantly at lower Damköhler numbers – they can, however, account for the observed effect of reduced apparent reactivity at higher Damköhler numbers.

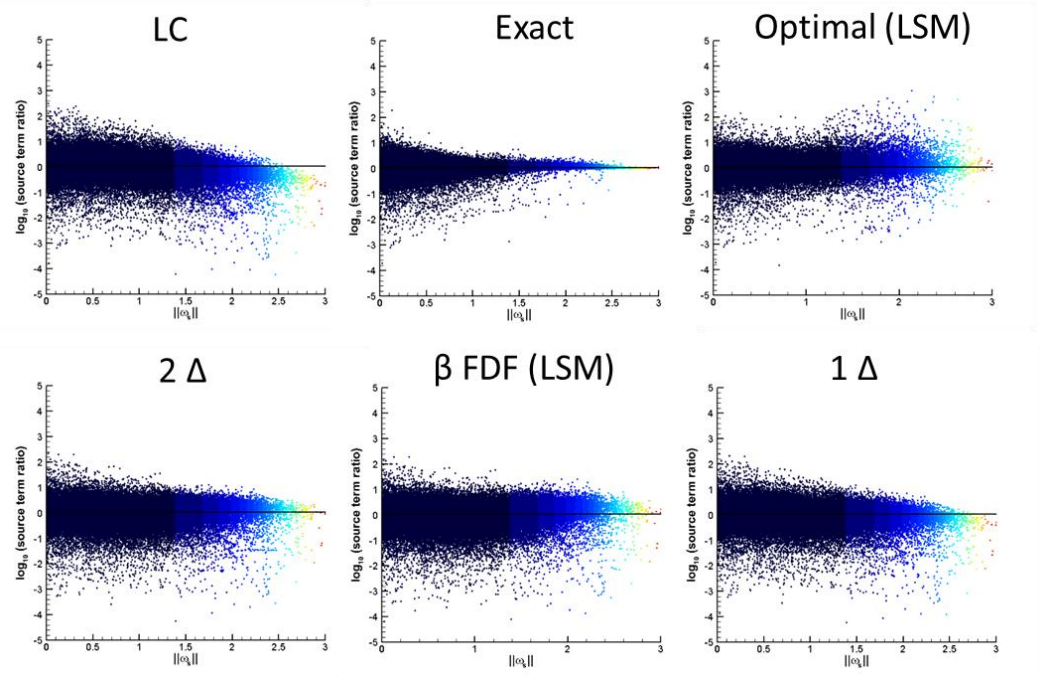

Figure 1: Scatterplots of production-rate norm ratios for different LSM models

Mesh-Sequenced Realizations for Evaluation of Subgrid-Scale Models for Turbulent Combustion

Jack R. Edwards[1] and Tanner B. Nielsen[2]
North Carolina State University, Raleigh, NC, 27695

This paper develops a new approach for analysis of subgrid closures for turbulent combustion as modeled using direct quadrature (finite-rate chemistry) techniques. The approach, termed Multi-Resolution Analysis through Mesh Sequenced Realizations (MRA-MSR) conducts simultaneous, constrained large-eddy simulations on a set of hierarcally-coarsened meshes. The availability of underlying fine-mesh (subgrid) data corresponding to coarse-mesh locations allows a clearer assessment of the effects of unresolved fluctuations on apparent reactivity. A key to MRA-MSR is the correlation of eddy structures at coarser mesh levels, which is facilitated by the transfer of filtered fine-mesh velocity information. Other means of constraining coarse-mesh species-production and subgrid turbulence transport can also be used. A seven-mesh MRA-MSR hierarchy using three resolution levels is applied to one of the Sydney bluff-body stabilized methane-hydrogen flames. Reasonable agreement with experimental data is achieved, though the results do show a marked sensitivity to the choice of outer boundary condition. Analysis of the simultaneously-evolved data at different resolution levels reveals several interesting trends. First, at high Damköhler numbers, there is clear evidence of attenuation of apparent reactivity due to the effects of unresolved fluctuations. At low Damköhler numbers, however, unresolved fluctuations can either diminish or enhance apparent reactivity. Secondly, single-point, single-time filtered density functions of a normalized subgrid Damköhler number show a characteristic beta PDF form and display evidence of scale similarity. Interrogation of the MRA-MSR database also shows that NCSU's Least Squares Minimization (LSM) turbulence / chemistry interaction model can account for the observed diminishment in reactivity at high Damköhler numbers but cannot reduce scatter significantly. A new form of the LSM model, which makes use of the normalized subgrid Damköhler number beta PDF distribution, performs slightly better than the original model, illustrating the potential of MRA-MSR in both assessing existing closure concepts and in developing new ones.

With burgeoning computing power, direct-quadrature (DQ) techniques for modeling turbulent combustion using large-eddy simulation have become more affordable. In contrast to tabulated-chemistry or eddy-dissipation methods, DQ techniques solve complete sets of rate equations for chemical production, strongly coupled with the evolving flow field. Typically, a flame structure will emerge during the course of a DQ calculation – one is not presumed as is common for tabulated-chemistry methods. As such, non-equilibrium processes such as flame extinction and flame lift can be captured naturally. Numerical challenges of DQ include the need to solve large systems of species conservation equations and the need to evaluate large numbers of rate equations describing multi-species chemical production at every time step. The latter can be circumvented by techniques such as ISAT [1], whereas the former, for implicit methods, can be addressed through decoupling or matrix-partitioning methods [2-4], which can yield *O(NS)* complexity. Modeling challenges relate firstly to the need to account for the influences of unresolved fluctuations on apparent reactivity as expressed at a given mesh level: $\overline{\dot{\omega}_s(q)} \neq \dot{\omega}_s(\bar{q})$. As flame structures captured using a DQ simulation are almost always under-resolved, there is also a first-order effect of numerical and modeled transport mechanisms on the obtained flowfield.

Many DQ techniques have been proposed over the years, ranging in complexity from 'laminar chemistry', in which chemical production terms are evaluated using filtered mean data alone, to algebraic techniques such as

[1] Professor, Department of Mechanical and Aerospace Engineering, Associate Fellow, AIAA
[2] Graduate Research Assistant, Department of Mechanical and Aerospace Engineering, Student Member, AIAA

simple PaSR strategies [5], thickened-flame models [6,7], and NCSU's least-squares minimization (LSM) models [8-10], to dual environment models (transport PaSR [11,12], DQMOM [13]), to LEM/ODT [14,15], in which the sub-grid reaction-transport problem is resolved very well but in only one spatial dimension, and finally, to Lagrangian / Eulerian FDF models [16,17], in which a number of independent realizations of the flow are performed and used to develop a statistical basis for a filtered-density function that describes the subgrid-scale PDF. While acceptable results have been achieved through all of these methods, there is no clear way to improve these models or to develop new ones that may be more adaptable and more in tune with today's computing power.

The purpose of this paper is to develop a framework, termed Multi-Resolution Analysis through Mesh Sequenced Realizations (MRA-MSR), that might be used as an analysis tool for the evaluation of existing SGS models for turbulent combustion and as a basis for constructing new models. The premise of MRA-MSR is that simultaneous, constrained realizations of a turbulent combusting flow at different resolution levels can be used to provide a clearer assessment of the effects of unresolved fluctuations. The method is developed as a general extension of classical *a priori* analysis, which has been used successfully to establish candidate closure forms for subgrid mass, momentum, and energy transfer in non-reactive systems and for reactive systems based on conserved-scalar approaches. In classical *a priori* analysis, data filtered from a DNS or a very fine LES is used as a 'truth model' to evaluate and improve SGS models. At some level in the process, principles of scale similarity are usually invoked, either for determining model forms or for establishing model 'constants'. While some attempts have been made to validate SGS models for filtered chemical production rates using this approach [18] using one-step chemistry, our experience is that the approach fails, in general, for detailed chemistry. The reason is as follows. The chemical and energy production rates, defined according to the law of mass action, may be split into production and depletion components:

$$\begin{aligned} &\dot{\omega}_s = \dot{\omega}_s^+ - \dot{\omega}_s^-; \\ &q = q^+ - q^- = \sum_s h_{0,s}^f \dot{\omega}_s^+ - \sum_s h_{0,s}^f \dot{\omega}_s^- \end{aligned} \tag{1}$$

The positive and negative components are nonlinear functions of temperature and composition, are often very large, and are generally close to one another in magnitude. The difference in the terms (the net production rate) is much smaller and is much more sensitive to small changes in composition and temperature than the positive / negative components. As a result, $|\overline{\dot{\omega}_s(q)}| << |\dot{\omega}_s(\bar{q})|$ in general, if the overbars represent the action of an explicit filtering operator. This leads to uncertain conclusions regarding the impact of SGS fluctuations on apparent reactivity as realized at a particular mesh level. MRA-MSR avoids this difficulty by evolving tandem large-eddy simulations on sequences of hierarchically coarsened meshes. The finest mesh (termed the 'parent') provides a source of local, instantaneous data that can be used to constrain solutions evolved on coarser meshes, primarily by forcing these solutions by the underlying fine-mesh velocity field. This correlates eddy structures but allows the reactive scalar fields on the coarser meshes to approach their equilibrium states in a more natural manner. A closer connection among reactive-scalar fields and functions thereof (such as chemical production and heat release rates) at different grid levels should emerge, making it possible to examine the impact of turbulence / chemistry interaction models in a less uncertain and more systematic manner.

An early version of MRA-MSR [8,9] used two mesh levels with solutions coupled through the velocity field. Calculations of high-speed turbulent diffusion flames were used to develop NCSU's LSM model [9,10], which embeds effects of sub-cell reactivity into a single flow-dependent scaling factor: $\overline{\dot{\omega}_s(q)} = f_{LSM}\,\dot{\omega}_s(\bar{q})$ (see section V subsection E for a more complete description of LSM). While LSM has been shown to provide a consistent (but in some cases modest) improvement in predictive capability, relative to 'laminar chemistry', it can fail (as can all models) in extreme situations – flame lift / stabilization / re-ignition, flame blowout, high rates of strain. A better database that delves deeper toward the DNS / resolved flame-structure limit is needed. This paper generalizes the two-level MRA-MSR to more than two levels (three levels tested so far) and incorporates additional ways of coupling the solutions across mesh levels. A user-specified number of realizations per mesh level can be specified, leading to hierarchies of simulataneous large-eddy simulations that can be data-mined to reveal new connections between measures of reactivity expressed at different scales.

The outline of this paper is as follows. First, details of the MRA-MSR framework are presented in Section II. The numerical methods employed in this study are then described in Section III, followed by details of the test case (one of the Sydney bluff-body stabilized flames) in Section IV. Results of this investigation and concluding remarks are presented in Sections V and VI, respectively.

I. MRA-MSR

A. MRA-MSR: Mesh Sequencing

The premise of MRA-MSR is that simultaneous, constrained realizations of a turbulent combusting flow at different resolution levels can be used to provide a clearer assessment of the effects of unresolved fluctuations. The starting point is a version of NCSU's REACTMB flow solver (Section III) constructed to evolve simultaneous solutions on a set of nested, structured, multi-block meshes. Each coarser mesh level is determined by removing every other mesh point of the next finest mesh level. Three nested mesh levels (coarse, medium, fine) can be used, and a user-specified number of realizations per mesh level can be evolved. Figure 1 (left) shows an example of a seven-mesh system, with one fine-mesh 'parent' communicating with three medium-mesh 'children' and three coarse-mesh 'children'. Figure 2 (right) shows a medium mesh 'parent' communicating with three coarse-mesh 'children' along with one independent coarse-mesh realization. Parallel processing is made easier by mapping each coarse-mesh block to the same processor as its fine mesh 'parent'. Information transfer between fine and coarse-mesh blocks is accomplished without MPI message-passing. It is possible to directly access finer-mesh information from a given coarse mesh level through various indexing rules. Given a coarse-mesh interior cell i,j,k, the eight cells on the medium mesh that lie 'within' this cell are those spanned by the index space 2i-2:2i-1, 2j-2:2j-1, 2k-2:2k-1. Likewise, the sixty-four cells on the fine mesh that lie 'within' this cell are those spanned by the index space 4i-6:4i-3, 4j-6:4j-3, 4k-6:4k-3. It is easy to see how one might identify and access the fine-mesh subgrid data that corresponds to a coarser-mesh location. Similar index mappings allow one to correlate data at cell interfaces, such as i+1/2,j,k. This allows the calculation of subgrid flux terms that correspond to a coarse-mesh cell interface, as discussed later.

B. MRA-MSR: Coupling

A key to MRA-MSR is correlation of turbulent eddy structures across mesh levels. Without this step, meaningful connections among the realizations cannot be achieved in an instantaneous sense. We achieve this by adding a relaxation source term to the momentum equations. The rate of relaxation is controlled by an estimated eddy-turnover time, which is related to an estimate of a turbulent mixing length provided by our LES/RANS model:

$$\frac{\partial \bar{\rho}\tilde{u}_i}{\partial t} + \frac{\partial(\bar{\rho}\tilde{u}_i\tilde{u}_j + \delta_{ij}\bar{p} - \tau_{ij,m} - \tau_{ij,sgs})}{\partial x_j} = \frac{1}{\tau}\bar{\rho}(\overline{u_{i,\,fine}} - \tilde{u}_i)$$

$$\frac{1}{\tau} = \frac{U_c}{\lambda_I}, U_c = 0.8U_a, \quad \lambda_I = C_I\lambda_{mix} \tag{2}$$

$$\lambda_{mix} = 1.5\sqrt{\frac{10\nu\bar{\omega} + \bar{k} + k_R}{C_\mu^{1/2}\bar{\omega}\bar{\omega}}}, \quad k_R = \underbrace{\frac{1}{2\bar{\rho}}\left(\overline{\bar{\rho}\tilde{u}_k\tilde{u}_k} - \frac{\overline{\bar{\rho}\tilde{u}_k}\,\overline{\bar{\rho}\tilde{u}_k}}{\bar{\rho}}\right)}_{\text{resolved TKE}}$$

The model constant C_I controls the rate of relaxation and is set to one for all cases presented herein. Also implemented are other means of constraining the solutions across mesh levels. Given a general volumetric filtering operator defined as

$$\overline{f(q)_{\text{fine}}} = \frac{\sum_k \Omega_k f(q_{k,\text{fine}})}{\sum_k \Omega_k} \tag{3}$$

where Ω_k is the cell volume, one can evaluate chemical production rates in several different ways:

$$\overline{\dot{\omega}_s} = \overline{\dot{\omega}_s(q)_{\text{fine}}} \quad \text{— Filtered source term}$$
$$\overline{\dot{\omega}_s} = \dot{\omega}_s(\overline{q_{\text{fine}}}) \quad \text{— Evaluation using filtered data from fine mesh}$$
$$\overline{\dot{\omega}_s} = \dot{\omega}_s(q_{\text{evolved, coarse}}) \quad \text{— Evaluation using evolved data from coarser mesh} \tag{4}$$

For coarse meshes, the first evaluation is expected to be the most accurate; the second, subject to much more error, and the third, somewhere between the two. The degree to which solutions constrained by each of these methods collapse toward one another is of interest, as it is a measure of mesh-independence in the absence of other factors.

In a similar manner, an 'exact' expression of subgrid scalar transport can be defined by filtering the underlying finer-mesh information:

$$\overline{\rho u_j'' \varphi''} = \overline{(\rho u_j \varphi)_{\text{fine}}} - \overline{(\rho u_j)_{\text{fine}}}\,\overline{(\rho \varphi)_{\text{fine}}} / \overline{(\rho)_{\text{fine}}} \tag{5}$$

Expressions such as these, applied to the species transport and energy equations on coarser meshes, can be used to replace modeled equivalents and can further constrain the solutions.

C. MRA-MSR: Protocol

A MRA-MSR calculation involves first the assembly of the mesh hierarchy and the initialization of the solutions on each mesh level. These initial solutions may be obtained from separate coarse-mesh calculations and then interpolated to the finer meshes or obtained from separate fine-mesh calculations and then filtered to the coarse meshes. Next, the constraint level for each mesh at every mesh level is defined. The finest mesh is assumed to be unconstrained; coarser meshes may be constrained or unconstrained. Velocity contraining is always employed, as discussed above. One can also contrain a particular coarse-mesh level by replacing species production source terms with those filtered from the underying fine-mesh solution. Using the index-notation analogue of Eq. 3 and assuming a fine-to-coarse transfer, we have, for example

$$\overline{\dot{\omega}_s(q)}|_{i,j,k} = \frac{\sum_{\hat{k}=4k-6}^{4k-3} \sum_{\hat{j}=4j-6}^{4j-3} \sum_{\hat{i}=4i-6}^{4i-3} \Omega_{\hat{i},\hat{j},\hat{k}} \dot{\omega}_s(q_{\hat{i},\hat{j},\hat{k}}|_{\text{fine}})}{\sum_{\hat{k}=4k-6}^{4k-3} \sum_{\hat{j}=4j-6}^{4j-3} \sum_{\hat{i}=4i-6}^{4i-3} \Omega_{\hat{i},\hat{j},\hat{k}}} \tag{6}$$

The third way that a solution can be constrained is by replacing modeled expressions for subgrid mass and energy transport with those calculated using direct filtering of the underlying fine-mesh data, per Eq. 5. Here, the filtering operation is applied at a coarse-mesh cell interface, such as i+1/2,j,k, illustrated below for a fine-to-coarse transfer of a generic variable ϕ:

$$\overline{\phi}|_{i+\frac{1}{2},j,k} = \frac{\sum_{\hat{k}=4k-6}^{4k-3} \sum_{\hat{j}=4j-6}^{4j-3} \sum_{\hat{i}=4i-4}^{4i-1} \Omega_{\hat{i},\hat{j},\hat{k}} \phi_{\hat{i},\hat{j},\hat{k}}|_{\text{fine}}}{\sum_{\hat{k}=4k-6}^{4k-3} \sum_{\hat{j}=4j-6}^{4j-3} \sum_{\hat{i}=4i-4}^{4i-1} \Omega_{\hat{i},\hat{j},\hat{k}}} \tag{7}$$

These choices are illustrated in Figure 1, where the abbreviations V, S, T correspond to constrained velocity, constrained source, and constrained transport. The solutions are then evolved at the same physical time step, with statistics taken as necessary using running time-averages. Fine-mesh time-averaged solutions can be filtered to the underlying coarse-mesh resolution for purposes of comparison.

II. Numerical Methods

The REACTMB flow solver from NCSU is used as the basis for this work. The REACTMB platform solves the compressible Navier-Stokes equations for reactive mixtures of gases on multi-block structured meshes using a finite-volume method. The inviscid fluxes are discretized using Edwards' Low Diffusion Flux-Splitting Scheme (LDFSS) [19] extended for operation at all Mach numbers using techniques described in [20]. The time advancement is fully implicit, using a second-order three-point backward time discretization. Sub-cycling techniques are used to converge the unsteady form of the governing equations to a prescribed tolerance at every physical time step. Incomplete LU (lower upper) factorization methods are used to solve the resulting linear system.

To extend the baseline first-order LDFSS method to higher-order, a hybrid strategy is employed. A MUSCL-type reconstruction of the primitive-variable vector $\vec{V} = [Y_1,....,Y_N, p, u, v, w, T, k, \omega]^T$ is used, where Y_k represents the kth species mass fraction. For all variables, a linear blend between a reconstructed variable (q) computed using a fourth-order central difference averaging operator and a limited variable computed using the Piecewise Parabolic Method is employed:

$$\begin{aligned} q_{L,i+1/2} &= q_{4th,i+1/2} + \beta_i (q_{L,ppm,i+1/2} - q_{4th,i+1/2}) \\ q_{R,i-1/2} &= q_{4th,i-1/2} + \beta_i (q_{R,ppm,i-1/2} - q_{4th,i-1/2}) \end{aligned} \tag{9}$$

The selection of the blending factor β differs based on the variable. For the scalars (mass fractions, pressure, temperature, turbulence variables), an essentially non-oscillatory function is utilized [21]:

$$\beta_i = \left(\frac{\| q_{i+1} - q_i | - | q_i - q_{i-1} \|}{| q_{i+1} - q_i | + | q_i - q_{i-1} | + 10^{-3} | q_i |} \right)^3 \tag{10}$$

For the velocities, a modified version of the Ducros switch [22] is used:

$$\beta_i = \frac{\max(\varepsilon^2, (\nabla \cdot \vec{V})^2)}{\max(\varepsilon^2, (\nabla \cdot \vec{V})^2) + (\nabla \times \vec{V}) \cdot (\nabla \times \vec{V})} \tag{11}$$

The limiting factor ε is selected as $\varepsilon = 5 \times 10^{-4} U_\infty / \max(\Delta x, \Delta y, \Delta z)_{field}$. This factor is problem-specific and is designed to ensure that the blending function approaches one in the free-stream and approaches zero in regions of high vorticity content.

REACTMB uses a hybrid LES/RANS closure initially developed by Gieseking, et al. [23]. For the cases discussed later, the RANS model (Menter's BSL) is active only very near the walls of the axisymmetric bluff body. A subgrid eddy viscosity due to Lenormand, et al. [24] is activated for the vast majority of the flow. Subgrid mass and energy transport is modeled using a gradient-diffusion strategy, parameterized by turbulent Schmidt (0.705) and Prandtl (0.9) numbers. Species viscosities are determined using Chemkin-type curve-fits, with mixture values determined using Wilke's law. Molecular diffusion is modeled using Fick's law, parameterized by a Schmidt number of 0.72. Heat conduction is modeled using Fourier's law, parameterized by a Prandtl number of 0.72. A synthetic-eddy method [25] is used to force turbulence at the inflow of the computational domain. This procedure requires a mean velocity and the Reynolds-stress tensor. The database for the Sydney flame (discussed later) is not detailed enough to provide all of this information, giving only the mean axial velocity and its rms value. Reynolds axial stresses are set to the square of the rms velocity, and the Reynolds shear stress is set to -1/2 of the Reynolds axial stress value. The chemical source terms are computed using the law of mass action. The test case discussed later involves combustion of a methane-hydrogen mixture – an 18-species 42-reaction model [26] is employed.

A finite-volume structured-mesh implementation of locally one-dimensional characteristics-based boundary conditions described in [27] is used in this study. By altering the level of 'known' information feeding in toward the domain, one can control the reflectivity characteristics of the boundary conditions. In the following, the subscript 'i' represents a cell just inside a boundary, the subscript 'g', a cell outside the boundary where the properties are to be evaluated, and the subscript 'f', the interface between these cells. The face area is denoted by A_k, the cell volume of the interior cell is Ω_i and $\vec{n}_k$ is the normal vector pointing in the direction of increasing coordinate index. The variable s is one if the face is a maximum index and zero if it is a minimum index. Given this, we first define signed wave speeds as follows:

$$
\begin{aligned}
&\lambda_1 = \vec{V}_i \cdot \vec{n}_k ; \lambda_1^+ = \max(0, \lambda_1); \lambda_1^- = \min(0, \lambda_1) \\
&\lambda_2 = \vec{V}_i \cdot \vec{n}_k + a_i ; \lambda_2^+ = \max(0, \lambda_2); \lambda_2^- = \min(0, \lambda_2) \\
&\lambda_3 = \vec{V}_i \cdot \vec{n}_k - a_i ; \lambda_3^+ = \max(0, \lambda_3); \lambda_3^- = \min(0, \lambda_3) \\
&\tilde{\lambda}_{1,2,3}^+ = s\lambda_{1,2,3}^+ - (1-s)\lambda_{1,2,3}^- \\
&\tilde{\lambda}_{1,2,3}^- = s\lambda_{1,2,3}^- - (1-s)\lambda_{1,2,3}^+
\end{aligned}
\tag{12}
$$

Given that

$$
\begin{aligned}
T_1 = \frac{1}{2\rho_i a_i} [& \tilde{\lambda}_2^+ (\Delta p + \rho_i a_i \Delta(\vec{U} \cdot \vec{n}_k)) + \tilde{\lambda}_2^- (\Delta p_0 + \rho_i a_i \Delta(\vec{U}_0 \cdot \vec{n}_k)) \\
& - \tilde{\lambda}_3^+ (\Delta p - \rho_i a_i \Delta(\vec{U} \cdot \vec{n}_k)) - \tilde{\lambda}_3^- (\Delta p_0 - \rho_i a_i \Delta(\vec{U}_0 \cdot \vec{n}_k))]
\end{aligned}
$$

the one-dimensional characteristic equations are then formulated as follows:

$$
\begin{aligned}
&\frac{\partial \vec{U}_g}{\partial t} + \frac{A_k}{\Omega_i} \left(T_1 \vec{n}_k + \tilde{\lambda}_1^+ (\Delta \vec{U} - \Delta(\vec{U} \cdot \vec{n}_k)\vec{n}_k) + \tilde{\lambda}_1^- (\Delta \vec{U}_0 - \Delta(\vec{U}_0 \cdot \vec{n}_k)\vec{n}_k) \right) = 0 \\
&\frac{\partial p_g}{\partial t} + \frac{A_k}{2\Omega_i} [\tilde{\lambda}_2^+ (\Delta p + \rho_i a_i \Delta(\vec{U} \cdot \vec{n}_k)) + \tilde{\lambda}_2^- (\Delta p_0 + \rho_i a_i \Delta(\vec{U}_0 \cdot \vec{n}_k)) \\
&\qquad + \tilde{\lambda}_3^+ (\Delta p - \rho_i a_i \Delta(\vec{U} \cdot \vec{n}_k)) + \tilde{\lambda}_3^- (\Delta p_0 - \rho_i a_i \Delta(\vec{U}_0 \cdot \vec{n}_k))] = 0 \\
&\frac{\partial \rho_{s,g}}{\partial t} - \frac{Y_{s,i}}{a_i^2} \frac{\partial p}{\partial t} + \frac{A_k}{\Omega_i} [\tilde{\lambda}_1^+ (\Delta \rho_s - \frac{Y_{s,i}}{a_i^2} \Delta p) + \tilde{\lambda}_1^- (\Delta \rho_{s,0} - \frac{Y_{s,i}}{a_i^2} \Delta p_0)] = 0 \\
&\frac{\partial k_g}{\partial t} + \frac{A_k}{\Omega_i} [\tilde{\lambda}_1^+ \Delta k + \tilde{\lambda}_1^- \Delta k_0] = 0 \\
&\frac{\partial \omega_g}{\partial t} + \frac{A_k}{\Omega_i} [\tilde{\lambda}_1^+ \Delta \omega + \tilde{\lambda}_1^- \Delta \omega_0] = 0
\end{aligned}
\tag{13}
$$

The formulation is completed by specifying Δq and Δq_0, where q is a fluid property. Δq is a finite difference taken to second order accuracy as $\Delta q = 1.5q_g - 2q_i + 0.5q_{i-1}$; $\Delta q_0 = k_q(q_\infty - q_g)$, which connects the 'g' state to a free-stream state located far away from the boundary. The property-specific relaxation coefficient k_q controls the degree to which the solution is constrained by the free-stream value. A non-reflecting (albeit in 1D) condition results if $k_q = 0$. In the results that follow, a value of $k_q = 0.002$ is prescribed for the pressure and velocity, with $k_q = 0.0$ used for all other variables. The equation system written above is solved for the 'g' cell values using a point-implicit sub-iteration method, fully coupled with the solution of the main flow equations.

III. Test Case

The test case considered in this investigation is one of the well-known Sydney bluff-body stabilized flames [28-30] (Figure 2). Many computational studies of the Sydney flames exist – good summaries may be found in [31] and [32]. The specific case used in this study is HM1E, which has a co-flow velocity of 35 m/s, a fuel jet velocity of 108 m/s, and uses a 50:50 (by volume) methane-hydrogen mixture. The bluff-body outer diameter is 50 mm and the fuel jet diameter is 3.6 mm. The experimental database is extensive, provding both velocity measurements (mean, Reynolds-stress components) and reactive scalar measurements (mean, rms). Mean and rms profiles for the co-flow velocity just upstream of the bluff-body face and the fuel jet velocity just downstream of the injection point

are available, as are estimates of the bluff-body face temperature. The co-flow velocity information was used in the synthetic-eddy model; the fuel-jet inflow was generated by solving for the flow within a small length of the fuel tube. The computational domain extends in the streamwise (X) direction from -36 mm (0.72 bluff-body diameters) to 375 mm (7.5 bluff-body diameters). The outer boundary of the cylindrical computational domain is located at a radius (R) of 90 mm (1.8 bluff-body diameters). Multi-block structured meshes were generated using GridGen; these meshes are clustered to the bluff-body walls and expand to nominal isotropic resolution between 0 mm (the bluff-body face) and 250 mm. The mesh is stretched in the axial direction downstream of X = 250 mm and is stretched in the radial direction away from R = 25 mm. Figure 1 shows centerplane details of the meshes employed. The finest mesh contains 102.6 M cells, the medium mesh contains 12.8 M cells, and the coarse mesh contains 1.60 M cells.

Three sets of calculations are discussed in this paper. The first set uses a seven-mesh hierarchy (1 fine 'parent', 3 medium constrained 'children', and 3 coarse constrained 'children'). A minimally-reflective boundary condition is imposed at the downstream X boundary, while a slip-surface boundary condition is imposed at the outer radial boundary. The second set uses the same seven-mesh hierarchy but utilizes a minimally-reflective boundary condition at the outer radial boundary. The third set uses a five-mesh hierarchy (1 medium 'parent', 3 coarse constrained 'children', 1 coarse independent realization) and also employs minimally-reflective boundary conditions at the downstream and radial boundaries. Seven-mesh hierarchies were evolved for a minimum of 6 combustor transit times, with statistics taken over ~3.5 combustor transit times. The five-mesh hierarchy was evolved for a longer period ~ 9 combustor transit times with statistics collected for 6.5 combustor transit times. All cases used a time step of 0.25×10^{-5} s.

IV. Numerical Results

A. Data Comparisons

Before proceeding with the MRA-MSR studies, it is useful to determine the degree of predictive capability offered by the baseline 'laminar chemistry' formulation for different mesh resolutions. Results from four independent realizations (Case 1: fine mesh with slip-surface outer boundary, Case 2: fine mesh with non-reflective outer boundary, Case 3: medium mesh with non-reflective outer boundary, and Case 4: coarse mesh with non-reflective outer boundary) are compared with one another and with experimental data in this section. A later section will focus on the *a priori* assessment of NCSU's LSM turbulence / chemistry interaction model using data extracted from the mesh hierarchy. Figure 3 shows time-averaged and instantaneous centerplane temperature profiles for each realization. Scales range from 300 K (black) to 2240 K (dark red). The influence of the outer boundary condition is highlighted strongly. With a slip-surface imposed at the outer boundary, disturbances generated from the wake-shedding process reflect, further energizing the shear layer, increasing entrainment rates, and generally shortening the recirculation region. Hot reaction products are trapped within the smaller recircuation region. When the minimally-reflecting conditions are imposed, these disturbances are transmitted through the outer radial boundary, leading to a less energized wake and a more elongated recirculation region. Peak flame temperature are located further downstream in this case. Medium and fine-mesh temperature predictions are comparable, but the fine-mesh result displays possible evidence of insufficient time-averaging. The fuel jet is predicted to be much less turbulent on the coarsest mesh and penetrates further downstream. The other cases predict similar jet penetration distances. Though not clearly indicated in these images, the effect of the synthetic-eddy generation process is minimal. The eddy structures generated fail to significantly energize the detaching shear layer.

Time-averaged predictions are compared with scalar measurements in Figures 4 and 5. Case 1 predictions are in black; Case 2, in red, Case 3, in blue, and Case 4, in green. The general structure of the mixing region is well-predicted, as evidenced by nitrogen mass fraction comparisons. Hydrogen and water concentration levels are also well predicted, but the kinetic processes that lead to CO_2 formation appear to be inhibited near the bluff body. This leads to a general excess of CO and a reduction in temperature in this region for all cases considered. It is not clear whether this trend is a result of the chemistry mechanism, insufficient mixing, excessive heat transfer to the bluff-body face, or to some combination of these factors. No case adequately predicts reactive-scalar behavior at the last station, which is near the point of maximum jet penetration. The flame is subject to high strain rates and highly intermittent behavior in this region.

Mean and rms axial velocity predictions are also shown in Figure 5. With the exception of the coarsest mesh prediction, which over-estimates the centerline axial velocity, mean velocity predicitons are in good accord with the experimental data. The turbulence intensity level is also well-predicted, except again for the coarsest mesh. A

close look at the rms data shows the effect of the reflective slip-surface boundary condition in increasing the turbulence intensity level in the free-stream.

Radial mean and rms velocity distributions are presented in Figure 6 along with Reynolds stress distributions. The coarse-mesh calculation underpredicts the peak radial mean velocity values as well as the rms value. A general improvement in the prediction of the rms radial velocity for the calculations performed on the finest mesh can also be seen. Reynolds stress predictions are in general agreement with experimental trends.

Taken as a whole, the level of predictive capability evidenced is within the range of other studies [31,32], which show similar deficiencies in the high-strain region and an inability to predict the correct jet penetration distance. The case is notably sensitive to the level of turbulence in the free-stream and in the outer part of the shear layer – the actual flame structure seems to be in between that predicted using a fully reflective and a minimally-reflective outer boundary condition. It is also probable that the fine-mesh results are not statistically converged. A major concern is the inability of the current framework to predict the CO to CO_2 conversion rate (and the associated temperature rise) near the bluff body. This is a subject of current study.

B. MRA-MSR: Effect of Constraints

The MRA-MSR framework allows one to constrain coarser-mesh solutions via the injection of underlying finer-mesh information. Velocity constraining is essential to correlate eddy structures; source and transport constraining can also be invoked. The seven-mesh hierarchy (Figure 1) uses velocity constraining, velocity+source constraining, and velocity+source+transport constraining applied to medium and coarse mesh levels. Figure 7 shows instantaneous and average centerplane temperature predictions for the case in which slip-surface outer boundary conditions are imposed. A strong correlation of eddy structures is observed, but the coarser-mesh results show the expected reduction in fine-scale content, which leads to some merging of thin reaction fronts into larger structures. Velocity coupling alone leads to an increase in average flame temperature as the mesh is coarsened. The addition of source-term constraining counteracts this effect, leading to reduced flame temperatures – cooler than the fine-mesh prediction. The effects of also constraining subgrid transport are not clear, as the source-term constraint appears to dominate. A disadvantage of source-term constraining is shown in Figure 8, which presents average CH_2O and CO mass fraction distributions along the centerplane. Radically different predictions emerge for CH_2O (and for other minor species, not shown) when fine-mesh source-term constraining is used. This indicates that these species do not achieve the correct partial equilibrium and/or steady states when forced by underlying fine-mesh information. The CO mass fraction distribution (and those of other major species) are not as affected.

C. MRA-MSR: Scatterplot Correlations

A major goal of the MRA-MSR framework is to discover influences of unresolved information on apparent reactivity as expressed at a particular mesh level. The availability of correlated finer-mesh information corresponding to every coarse-mesh location enables analyses that may be used to quantify these influences. Figure 9 shows a map of 585 coarse-mesh cells for which information has been extracted. For each coarse-mesh cell, we output flow properties from the cell itself and from the 26 face / edge / vertex neighbors of the cell. Underlying medium-mesh (8 × 27 cells) and fine-mesh (64 × 27 cells) information within this neighborhood is also outputted. Fine-to-medium and fine-to-coarse velocity scatterplots are shown in Figure 10 for different coarse-mesh constraints. The seven-mesh hierarchy calculation that employs the reflective slip-surface boundary condition provides the database. Here, the volumetric filtering operation defined in Eqs. 3 and 6 is applied to the finer-mesh data The velocity scatterplots show a linear slope with small variance – a reflection of the tight correlation of eddy structures facilitated by Eq. 2. The level of variance increases substantially for the temperature, as shown in Figure 11, though the correlation remains nearly linear. More scatter is evidenced for the fine-to-coarse interaction than for the fine-to-medium interaction, and the inclusion of source contraining and source + transport constraining appears to reduce the variance in the distributions somewhat.

Correlations of measures of reactivity require different methods of analysis. As discussed earlier, while 'positive' and 'negative' components of chemical production terms might individually exhibit a similar level of correlation with decreasing mesh resolution (but with more scatter), small changes in reactive-scalar data can easily shift the positive / negative component balance, leading to large changes in the net production rate. We first define an L_2 norm of the source-term vector in the usual manner: $\| \dot{\omega} \| = (\sum_s \dot{\omega}_s \dot{\omega}_s)^{1/2}$. We then take the ratio of the norm

filtered from a fine mesh to that evaluated using data evolved on a coarser mesh (a subgrid model could be applied at this point) as a measure of the effect of unresolved fluctuations on apparent reactivity:

$$R = \frac{\| \overline{\dot{\omega}(q_{fine})} \|}{\| \overline{\dot{\omega}(q_{evolved,coarse})}_{\mathrm{mod}} \|} \tag{14}$$

If R is less than one, unresolved fluctuations act to diminish local reactivity; if R is greater than one, the opposite is true. The next set of results consider $\| \overline{\dot{\omega}(q_{evolved,coarse})} |_{\mathrm{mod}} \| = \| \dot{\omega}(q_{evolved,coarse}) \|$ (the laminar chemistry assumption); velocity constraining alone is utilized. Figure 12 plots the base-10 logarithm of R versus a subgrid Damköhler number for fine-to-coarse, fine-to-medium, and medium-to-coarse interactions. A close-up view of one interaction is shown in Figure 13. The subgrid Damköhler number is defined as

$$Da = \frac{\| \dot{\omega}(q_{evolved,coarse}) / \rho(q_{evolved,coarse}) \| \Delta^2}{\max(\nu_{evolved,coarse}, u'_{sgs} \Delta)}, \tag{15}$$

In this expression, the kinematic viscosity and density are evaluated using the data evolved on the coarser mesh. The filter width is taken to be the cube root of the coarser-mesh cell volume, and the subgrid fluctuation velocity is calculated from the underlying finer mesh solution as follows:

$$u_{sgs} = \sqrt{\frac{1}{2}(\overline{u^2} - \bar{u}^2 + \overline{v^2} - \bar{v}^2 + \overline{w^2} - \bar{w}^2)}\,, \tag{16}$$

where the volumetric filtering operations (Eqs. 3 and 6) are again employed. Scatterplot symbols are colored and sized by Damköhler number. The pink region corresponds to attenuation, while the solid black line indicates the R = 1 neutral point, at which unresolved fluctuations neither attenuate nor augment local reactivity. Several trends can be noted. First, the degree of scatter about the neutral point decreases for the fine-to-medium interaction relative to the fine-to-coarse or medium-to-coarse interactions. This is as expected, as more of the flame structure is resolved on the medium mesh. Secondly, the degree of scatter increases substantially at low Damköhler numbers – attenuation appears equally as probable as augmentation. As the Damköhler number increases, however, all interactions display a clear trend toward inhibition of reactivity, with the fine-to-coarse interaction being the most prominent example. As noted in Figure 13, a perfect subgrid closure would completely collapse the data about the neutral point. It appears plausible that a relatively simple subgrid model could counteract the downward shift of the distribution at higher Damköhler numbers, thus modeling the inhibition effect, but reducing the scatter, especially at lower Damköhler numbers, might be much more difficult. We will return to this conjecture later.

D. MRA-MSR: Filtered Density Functions

The output from MRA-MSR can be used to form single-point, single-time filtered density functions (FDFs). It is of interest to determine how such FDFs might be correlated among mesh levels. Subgrid statistics of conserved scalars are a cornerstone of many turbulent combustion models – the subgrid FDF of the mixture fraction, for example, is often modeled using a beta PDF. A question is whether subgrid FDFs of measures of SGS reactivity could be extracted, and if so, what characteristic forms they might possess. Though others could be chosen, the quantity selected for study is a normalized Damköhler number, defined over a neighborhood surrounding a particular mesh point as follows:

$$\begin{aligned} \overleftrightarrow{\mathrm{Da}}_{\mathrm{k}} &= \frac{\mathrm{Da}_{\mathrm{k}} - \mathrm{Da}_{\mathrm{min}}}{\mathrm{Da}_{\mathrm{max}} - \mathrm{Da}_{\mathrm{min}}}, \mathrm{Da}_{\mathrm{k}} = \frac{\| \dot{\omega}(q_k) / \rho_k \| \Delta^2}{\max(\nu, u'_{sgs} \Delta)} \\ \mathrm{Da}_{\mathrm{min}} &= \min(\mathrm{Da}_{\mathrm{k}}) |_{k=\mathrm{neighborhood}}, \\ \mathrm{Da}_{\mathrm{max}} &= \max(\mathrm{Da}_{\mathrm{k}}) |_{k=\mathrm{neighborhood}} \end{aligned} \tag{17}$$

As the scaling factor (the term multiplying the production-rate norm) is independent of the location within the neighborhood, the normalized Damköhler number metric essentially orders the distribution of inverse chemical time scales within the neighborhood from smallest to largest (zero to one in the normalized space).

Several examples of the FDF of the normalized Damköhler number are shown in Figure 14. These are extracted from the underlying fine-mesh reactive-scalar data (64 cells) corresponding to coarse-mesh cells located at different points within the domain at different times. Eight 'bins' are used to develop the discrete FDF; also shown is a beta PDF distribution calculated using subgrid mean and variance information extracted from the neighborhood.

The beta PDF distribution performs quite well in capturing the trends of the discrete distribution. This rather surprising result might be explained by the fact that the non-premixed nature of the Sydney flame lends itself (to a first degree of approximation) to a flamelet-type formulation in which instantaneous reactive scalars are directly mapped to the mixture fraction.

To determine whether the extracted single-point FDFs show evidence of scale-similarity, the neighborhood of data surrounding each spatial location must be expanded so that viable FDFs can be calculated at the coarsest-mesh level. The entire data-extraction neighborhood (27 coarse-mesh locations, 8×27 medium-mesh locations; 64×27 fine-mesh locations) is thus used, and again, eight 'bins' are used to develop the discrete FDFs. Figure 15 shows several examples of FDFs extracted from the different meshes. Even given the sparsity of the coarse-mesh data neighborhood, strong evidence of scale-similarity can be noted, and again, a beta PDF form provides a reasonable model for the calculated distributions. This result shows that the form of the subgrid FDF of the normalized Damköhler number might be reasonably approximated by interrogation of the neighborhood of data surrounding a particular spatial location, raising the possibility of constructing scale-similarity-based closures for turbulence / chemistry interactions.

E. MRA-MSR: SGS Closure Analysis

The MRA-MSR framework can also be used to conduct *a priori* analyses to identify the particular effects of selected turbulence / chemistry interaction models. We return to NCSU's LSM model, which embeds effects of sub-cell reactivity into a single flow-dependent scaling factor: $\overline{\dot{\omega}_s(q)} = f_{LSM}\,\dot{\omega}_s(\overline{q})$, with

$$f_{LSM} = \frac{\sum_s \overline{\dot{\omega}_s(q)}|_{\mathrm{mod}}\,\dot{\omega}_s(\overline{q}) + A^2\,|\sum_s h^f_{0,s}\,\overline{\dot{\omega}_s(q)|_{\mathrm{mod}}}\,|\,|\sum_s h^f_{0,s}\dot{\omega}_s(\overline{q})|}{\sum_s \dot{\omega}_s(\overline{q})\dot{\omega}_s(\overline{q}) + A^2(\sum_s h^f_{0,s}\dot{\omega}_s(\overline{q}))^2}, \qquad A = \left\{ \begin{array}{c} 0 \\ 1/\sum_k Y_k C_{p,k}(\tilde{T})\tilde{T} \end{array} \right\} \begin{array}{c} \\ \text{or} \end{array} \tag{18}$$

Different LSM model variants can be defined through different choices of $\overline{\dot{\omega}_s(q)}|_{\mathrm{mod}}$. LSM-FS (filtered source) sets

$$\overline{\dot{\omega}_s(q)}|_{\mathrm{mod}} = \mathrm{sgn}(\dot{\omega}_s(\overline{q}))\,|\sum_k \alpha_k \dot{\omega}_s(\overline{q}_k)| \tag{19}$$

with the sum taken over the members of the neighborhood and the weights α_k are chosen to approximate a filtering operation at the Δ or 2Δ level. LSM-exact sets

$$\overline{\dot{\omega}_s(q)}|_{\mathrm{mod}} = \mathrm{sgn}(\dot{\omega}_s(\overline{q}))\,|\overline{\dot{\omega}_s(q)}|, \tag{20}$$

which requires filtering of the underlying fine-mesh production terms. A final variant, motivated by the FDF analysis described above and termed LSM-FDF, sets

$$\overline{\dot{\omega}_s(q)}|_{\mathrm{mod}} = \mathrm{sgn}(\dot{\omega}_s(\overline{q}))\,|\int_{\overleftrightarrow{Da}} \dot{\omega}_s(\overleftrightarrow{\mathrm{Da}})\beta(\overleftrightarrow{\mathrm{Da}})d[\overleftrightarrow{\mathrm{Da}}]\,| \equiv \mathrm{sgn}(\dot{\omega}_s(\overline{q}))\,|\sum_k \beta_k \dot{\omega}_s(\overline{q}_k)|\,, \tag{21}$$

The implementation of this approach requires first a sorting of the members of the neighborhood in order of increasing normalized Damköhler number and then the application of a discrete quadrature using a beta PDF expressed as a function of the neighborhood mean and variance. This information may be obtained through interrogation of the resolved-scale neighborhood to achieve a self-contained closure, or, in the MRA-MSR context, calculated from the underlying fine-mesh data. In either case, the result is a different set of weighting factors β_k used in the sum over neighborhood members.

Returning to the analysis of source-term norm ratios, R is now defined as

$$R = \frac{\|\,\overline{\dot{\omega}(q_{fine})}\,\|}{\|\,f_{LSM}\,\dot{\omega}(q_{evolved,coarse})\,\|}, \tag{22}$$

where f_{LSM} is computed using each of the formulations mentioned above. Figures 16 and 17 show the results for fine-to-coarse and fine-to-medium interactions, with A in Eq. 18 set equal to zero. LSM-exact, by construction, collapses the data about the R=1 neutral point for both interactions, as $f_{LSM-exact}$ is the least-squares solution to the minimization problem $\min_f [\sum_s (\overline{\dot{\omega}_s(q)} - f\dot{\omega}_s(\bar{q}))^2]$. For the fine-to-coarse interaction, LSM-FS begins to shift the data toward the neutral point; LSM-FDF further shifts the data, but neither reduces the scatter significantly. Similar trends are displayed for the fine-to-medium interaction. In this case, LSM-FDF starts to over-correct for the attenuation effect, while LSM-FS centers much of the distribution about the neutral point. These results show the potential of the LSM models in correcting for the attenuative effects of unresolved fluctuations at high Damköhler numbers but also indicate a modest sensitivity to the mesh size. The fact that none of the LSM models (except for the 'exact' one) reduces the scatter significantly indicates that a simple linear scaling of the laminar-chemistry production term may not possess the necessary degrees of freedom to account for complicated subgrid effects, especially those occurring at lower Damköhler numbers. The more important point is that the MRA-MSR framework can be used both to assess the general potential of various closure forms for turbulence-chemistry interactions and to develop new closure forms (the LSM-FDF variant being one example).

V. Conclusions

A new method for evaluating subgrid closures for large-eddy simulation of turbulent combustion, termed Multi-Resolution Analysis through Mesh Sequenced Realizations (MRA-MSR), has been proposed and tested in this work. The premise of MRA-MSR is that simultaneous, constrained large-eddy simulations performed on hierarchies of successively coarsened meshes can provide a means of connecting reactive scalar information at different scales of resolution. The approach is potentially an improvement over classical *a priori* analysis as a means of evaluating and developing subgrid closures for strongly non-linear and intermittent functions, such as chemical species production rates. MRA-MSR requires firstly a means of constraining eddy structures on coarser meshes so that they are strongly correlated with structures evolved on finer meshes; this is accomplished through a velocity-relaxation term added to the coarse-mesh momentum equations. Other methods of constraining coarse-mesh solutions include the replacement of chemical production rates with those filtered from the underlying fine mesh and the construction of 'exact' forms for subgrid mass, momentum, and energy transport based on the underlying fine-mesh data.

MRA-MSR has been applied to one of the Sydney bluff-body stabilized methane-hydrogen flames using a three-mesh hierarchy with the finest mesh containing ~108 M cells. Comparisons with experimental scalar and velocity data show generally good agreement with measured trends, with the most noteworthy deficiencies being an inaccurate prediction of the maximum fuel jet penetration distance and a reduced rate of CO to CO_2 conversion near the face of the bluff body. The predictions at all mesh levels are sensitive to the imposed outer boundary condition, with a reflective slip-surface boundary condition resulting in higher levels of fluctuation intensity in the recirculation region. The use of a minimally-reflective boundary condition reduces the turbulence intensity, leading to a more elongated recirculation zone. The structure of the actual flame seems to be bracketed by these values.

The inclusion of chemical-source constraining for the coarser meshes cools the predicted flame, compared with the use of velocity-constraining alone. Radical-species distributions are disrupted when chemical-source constraining is used - partial equilibrium and/or steady states for these appear to be incorrectly predicted. These results indicate that it may be of no advantage to constrain coarse-mesh solutions with information other than the velocity.

An analysis of reactive-scalar behavior at different mesh resolution levels reveals several interesting trends. Scatterplot correlations for reactive scalars show substantial increases in variance with decreases in resolution level. Correlations between chemical production terms filtered from the fine mesh to those constructed using evolved coarse-mesh data show further increases in variance but reveal a clear trend of diminishing apparent reactivity due to unresolved fluctuations at high subgrid Damköhler numbers. Single-point, single-time filtered density functions of a locally normalized subgrid Damköhler number (a measure of the distribution of inverse chemical time scales in the neighborhood of a particular spatial location) show a characteristic beta-PDF form and display a large degree of scale similarity. This result provides support for the use of scale-similarity ideas in formulating closures for subgrid turbulence / chemistry interactions.

MRA-MSR can be used to conduct *a priori* evaluations of the potential effects of selected closures for turbulence-chemistry interactions. As an example, several variants of NCSU's Least-Squares Minimization (LSM) model have been evaluated using the MRA-MSR three-mesh database. A new LSM variant which averages chemical source terms over the neighborhood using a beta PDF distribution based on the normalized Damköhler

number has been developed, based on the results discussed above. Both this variant and one that conventionally filters chemical source terms show promise in capturing the generally diminishing effect of subgrid fluctuations on apparent reactivity but fail to reduce the scatter significantly. This result indicates that LSM might not possess enough degrees of freedom to model very complicated subgrid effects, particularly those occurring at low Damköhler number.

Acknowledgments

This work is supported by the Army Research Office, under Short Term Innovative Research grant W911NF-17-1-0074, monitored by Dr. Ralph Anthenien. Computer time was obtained from the DoD's HPCMP program, with access facilitated by Dr. Joseph Myers (ARO) and Mr. David Dumas (ERDC).

References

[1] Pope, S.B. "Computationally Efficient Implementation of Combustion Chemistry using In Situ Adaptive Tabulation", *Combust. Theor. Model.* 1, 41-63, 1997.
[2] Candler, G., Subbareddy, P., and Nompelis, I. "Decoupled Implicit Method for Aerothermodynamics and Reacting Flows" *AIAA Journal*, Vol. 51 No. 5, pp. 1245-1254, 2013.
[3] Savard, B., Xuan, Y. Bobbitt, B., Blanquart, G. "A Computationally-Efficient, Semi-Implicit, Iterative Method for the Time-Integration of Reacting Flows with Stiff Chemistry, J. *Comp. Phys*, 295, 740-769, 2015.
[4] Nielsen, T., Edwards, J., Chelliah, H., Lieber, D., Goyne, C., Rockwell, R., and Cutler, A. "Numerical Simulation of Supersonic Premixed Turbulent Combustion" AIAA-2017-0601, 2017.
[5] Berglund, M., Fedina, E., Fureby, C. and Tegner, J. "Finite Rate Chemistry Large-Eddy Simulation of Self-Ignition in a Supersonic Combustion Ramjet," *AIAA J.*, 48, 540-550, 2010.
[6] Colin, O., Ducros, F., Veynante, D., and Poinsot, T. "A Thickened Flame Model for Large Eddy Simulations of Turbulent Premixed Combustion," *Phys. Fluids*, 12, 1843-1863, 2000.
[7] Charlette, F., Meneveau, C., and Veynante, D. "A Power-Law Flame-Wrinkling Model for LES of Premixed Turbulent Combustion Part II: Dynamic Formulation," *Combust. Flame*, 131, 181-197, 2002.
[8] Patton, C., Wignall, T., Mirgolbabaei, H., Edwards, J.R., and Echekki, T. "LES Model Assessment for High Speed Combustion using Mesh Sequenced Realizations" AIAA Paper 2015-4207, 2015.
[9] Patton, C.H., Wignall, T.J., Edwards, J.R., and Echekki, T. "LES Model Assessment for High-Speed Combustion", AIAA Paper 2016-1937, 2016
[10] Potturi, A., Patton, C.H., and Edwards, J.R "Application of Data-Driven SGS Turbulent Combustion Models to the Volvo Experiment", AIAA Paper 2017-1792, 2017.
[11] Sabelnkov, V. and Fureby, C. "Extended LES-PASR Model for Simulation of Turbulent Combustion," *Prog. Propuls. Phys*., 4, 539-568, 2013.
[12] Potturi, A. and Edwards, J. "Investigation of Subgrid Closure Models for Finite-Rate Scramjet Combustion," AIAA Paper 2013-2461, 2013.
[13] Koo, H., Donde, P. and Raman, V. "A Quadrature-Based LES/Transported Probability Density Function Approach for Modeling Supersonic Combustion," *Proc. Combust. Inst*., 33 2203-2210, 2011.
[14] Menon, S., McMurtry, P. A, and Kerstein, A. R., "A Linear Eddy Subgrid Model for Turbulent Combustion - Application to Premixed Combustion," AIAA Paper 1993-0107, 1993.
[15] Echekki, T., Kerstein, A.R., and Dreeben, T.D., "One Dimensional Turbulence Simulation of Turbulent Jet Diffusion Flames: Model Formulation and Illustrative Applications," *Combust. Flame*, 125, 1083-1105, 2001.
[16] Jaberi, F.A., Colucci, P.J., James, S., Givi, P., and Pope, S.B. "Filtered Mass Density Function for Large-Eddy Simulation of Turbulent Reacting Flows," *J. Fluid Mech*., 401, 85-121.,1999
[17] Valino, L. "A Field Monte Carlo Formulation for Calculating the Probability Density Function of a Single Scalar in a Turbulent Flow, " *Flow Turbulence Combust*., 60, 157-172, 1998.
[18] DesJardin, P. and Frankel, S. "Large Eddy Simulation of a Nonpremixed Reacting Jet: Application and Assessment of Subgrid-Scale Combustion Models, *Phys. Fluids*, 10, 2298-2314, 1998.
[19] Edwards, J. "A Low-Diffusion Flux-Splitting Scheme for Navier-Stokes Calculations," *Comput. Fluids*, 26, 635-659, 1997.
[20] Edwards, J. "Towards Unified CFD Simulations of Real Fluid Flows," AIAA Paper 2001-2524, 2001.
[21] Normal, M., Semazzi, F., and Nair, R., "Conservative Cascade Interpolation on the Sphere: an Intercomparison of Various Non-Oscillatory Reconstructions," *Q.J.R. Meteorol. Soc*., 135, 795-805, 2009.

[22] Ducros, F., Ferrand, V., Nicaud, F., Weber, C., Darracq, D., Gachareiu, C., and Poinsot, T. "Large-eddy simulation of the shock / turbulence interaction", *Journal of Computational Physics*, Vol. 152, No. 2, 517-549, 1999.
[23] Gieseking, D., Choi, J., Edwards, J., and Hassan, H. "Compressible Flow Simulations Using a New Large-Eddy Simulation / Reynolds-Averaged Navier-Stokes Model." *AIAA J.*, 49, 2194-2209, 2011.
[24] Lenormand, E., Sagaut, P., Ta Phuoc, L., and Compte, P. "Subgrid-Scale Models for Large-Eddy Simulations of Compressible Wall-Bounded Flows," *AIAA J.*, 38, 1340-1350, 2000.
[25] Jarrin, N., Benhamadouche, S., Laurence, D., and Prosser, R. "A Synthetic-Eddy Method for Generating Inflow Conditions for LES," *Int. J. of Heat and Fluid Flow*, 27, 585-593, 2006.
[26] Larsson, A., Zettervall, N., Hurtig, T., Nilson, E.J.K., Ehn, A., Petersson, P., Alden, M., Larfeldt, J., and Fureby, C. "Skeletal Methane-Air Reaction Mechanism for Large-Eddy Simulation of Turbulent Microwave-Assisted Combustion," *Energy Fuels*, DOI: 10.1021/acs.energyfuels.6b02224, Jan, 2017.
[27] Pirozzoli, S. and Colonius, T. "Generalized Characteristic Relaxation Boundary Conditions for Unsteady Compressible Flow Simulations," *J. Comp. Physics*, Vol. 248, 109-126, 2013.
[28] Masri, A.R., Dally, B.B., Barlow, R.S. and Carter, C.D., "The Structure of The Recirculation Zone of a Bluff-Body Combustor," Twenty-fifth Symposium (International) on Combustion, The Combustion Institute, Pittsburgh, 1994, pp.1301-1308.
[29] Masri, A.R., Dibble, R.W., and Barlow, R.S., "The Structure of Turbulent Nonpremixed Flames Revealed by Raman-Rayleigh-LIF Measurements," *Prog. Energy Combust. Sci*., 22, 307-362, 1997.
[30] http://web.aeromech.usyd.edu.au//thermofluids/bluff.htm
[31] Olbricht, C., Ketelheun, A., Hahn, F., and Janicka, J. "Assessing the Predictive Capabilities of Combustion LES as Applied to the Sydney Flmae Series," Flow Turbulence Combust. 85,513-547, 2010.
[32] Kempf, A.M., Geurts, B.J., Oefelein, J.C. "Error Analysis of Large-Eddy Simulation of the Turbulent Non-Premixed Sydney Bluff-Body Flame," U.S. Department of Energy Publications, 116, , 2011.

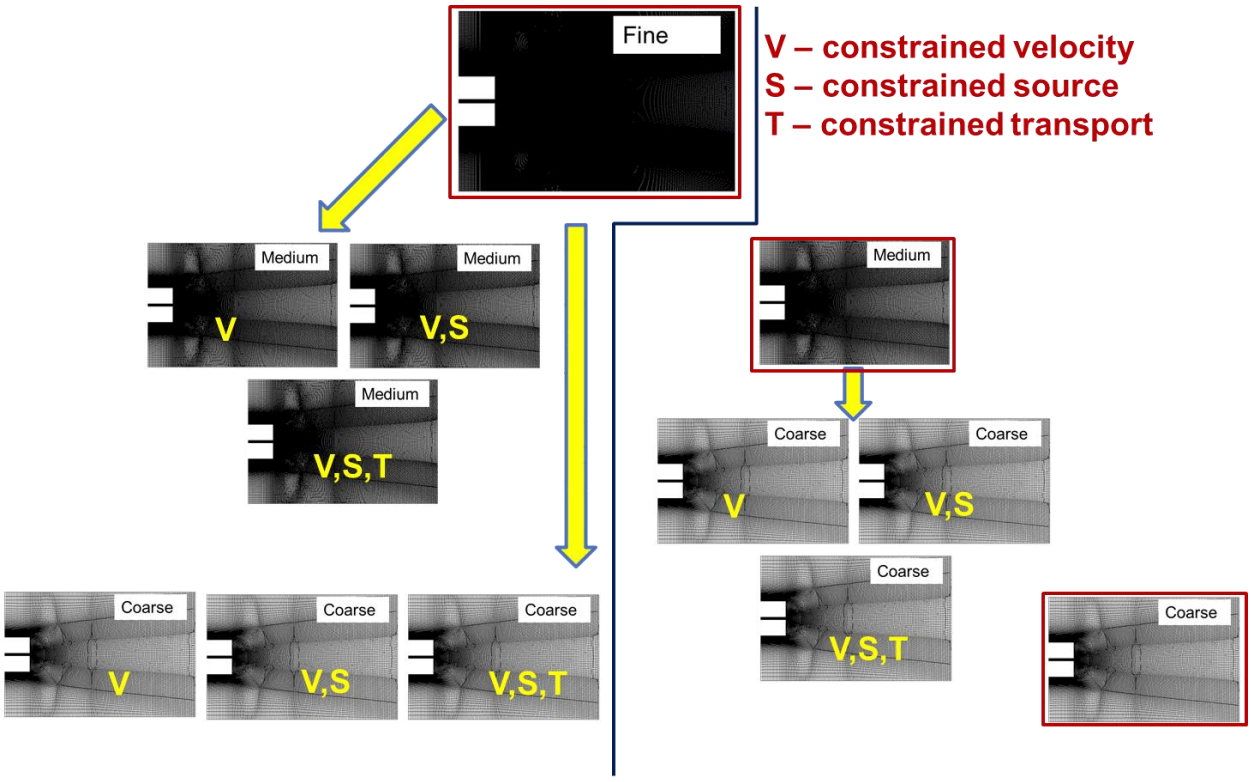

Figure 1. Mesh hierarchy for MRA-MSR (left branch: three-level, seven-mesh system; right branch; two-level, five-mesh system)

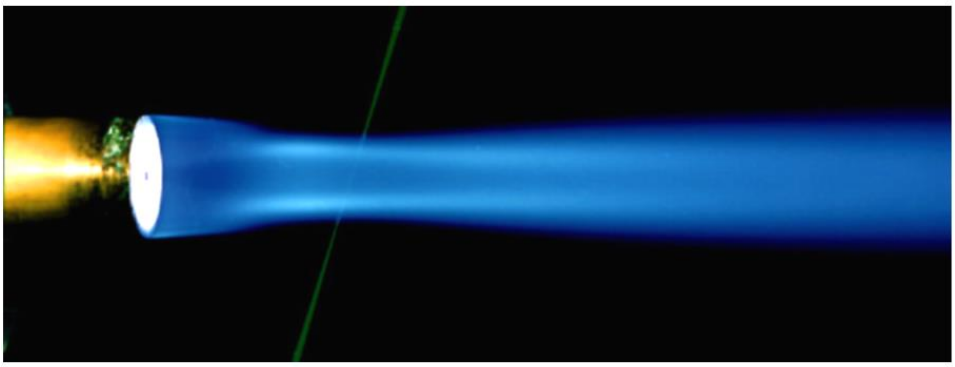

Figure 2. Image of Sydney bluff-body stabilized flame (http://web.aeromech.usyd.edu.au//thermofluids/bluff.htm)

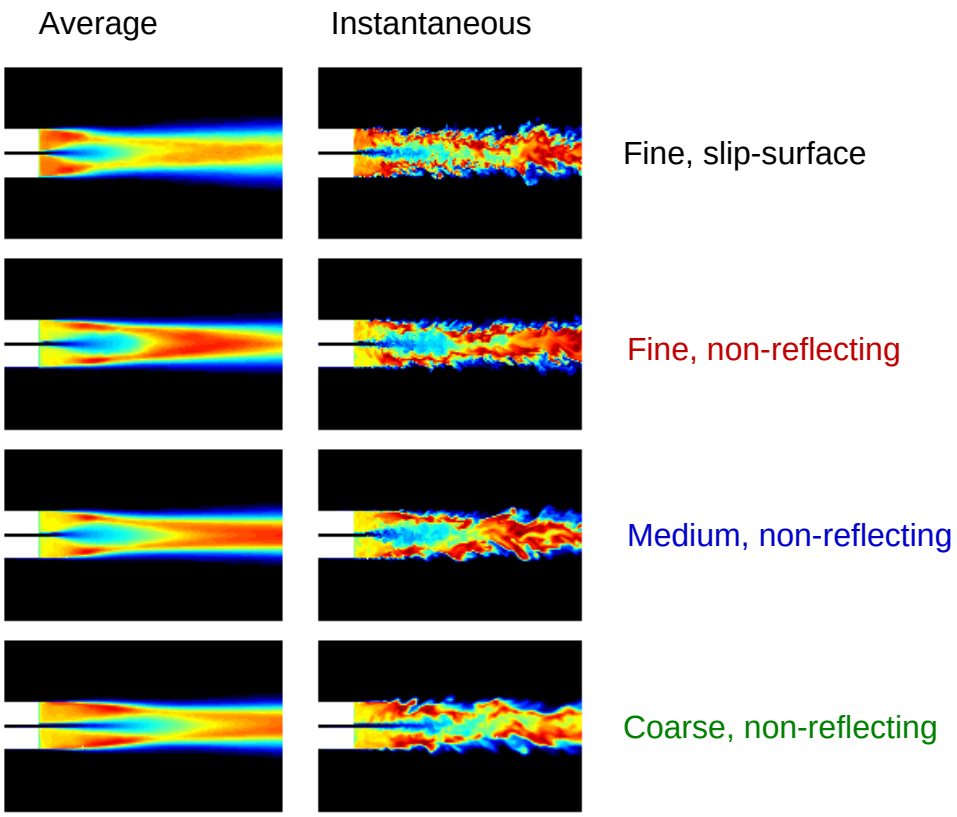

Figure 3. Average and instantaneous centerline temperature distributions (unconstrained realizations on fine, medium, and coarse meshes)

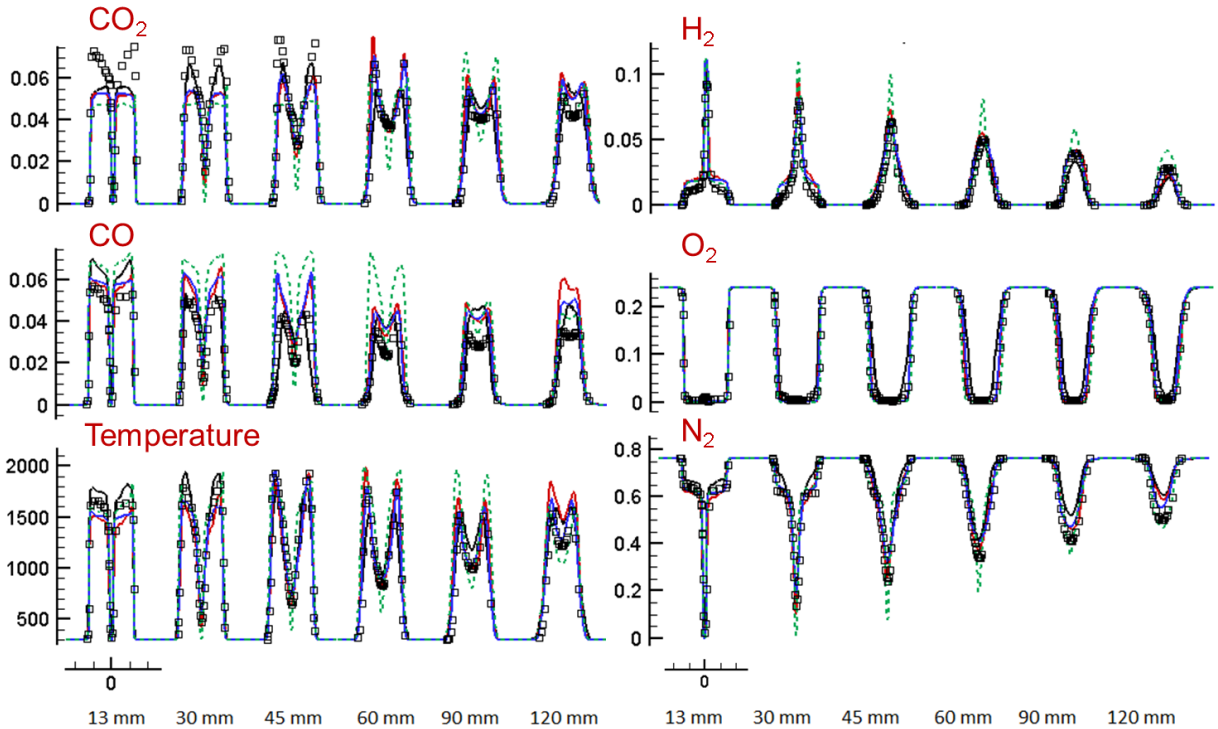

Figure 4: Comparisons with mean scalar measurements

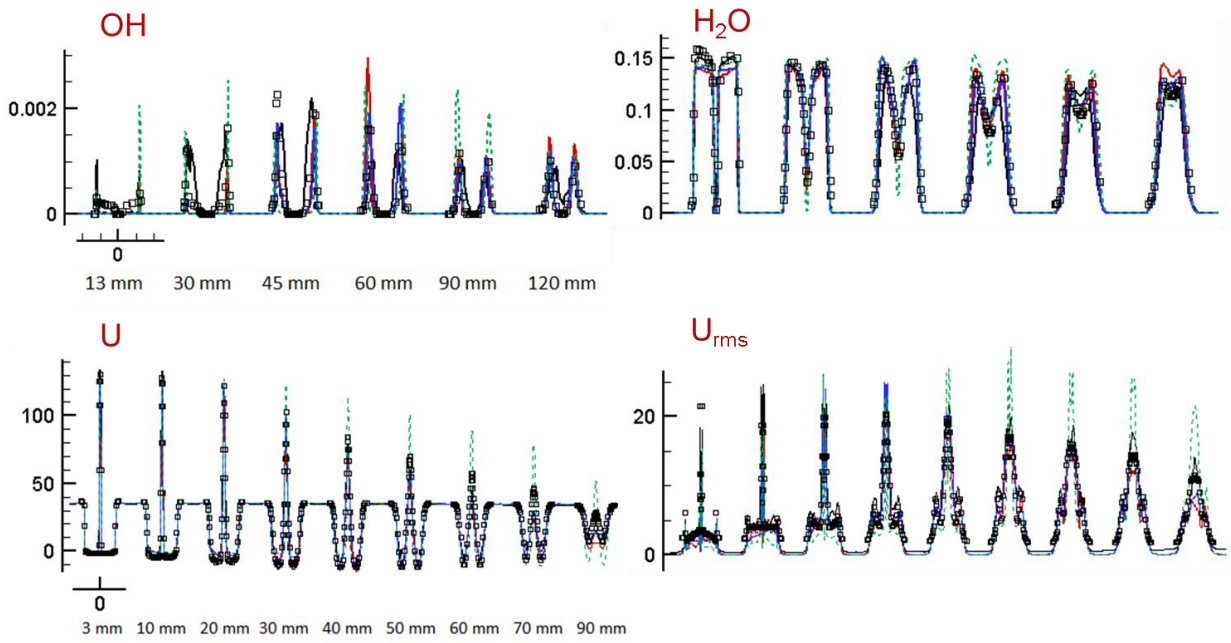

Figure 5: Comparisons with mean scalar and mean and rms axial velocity measurements.

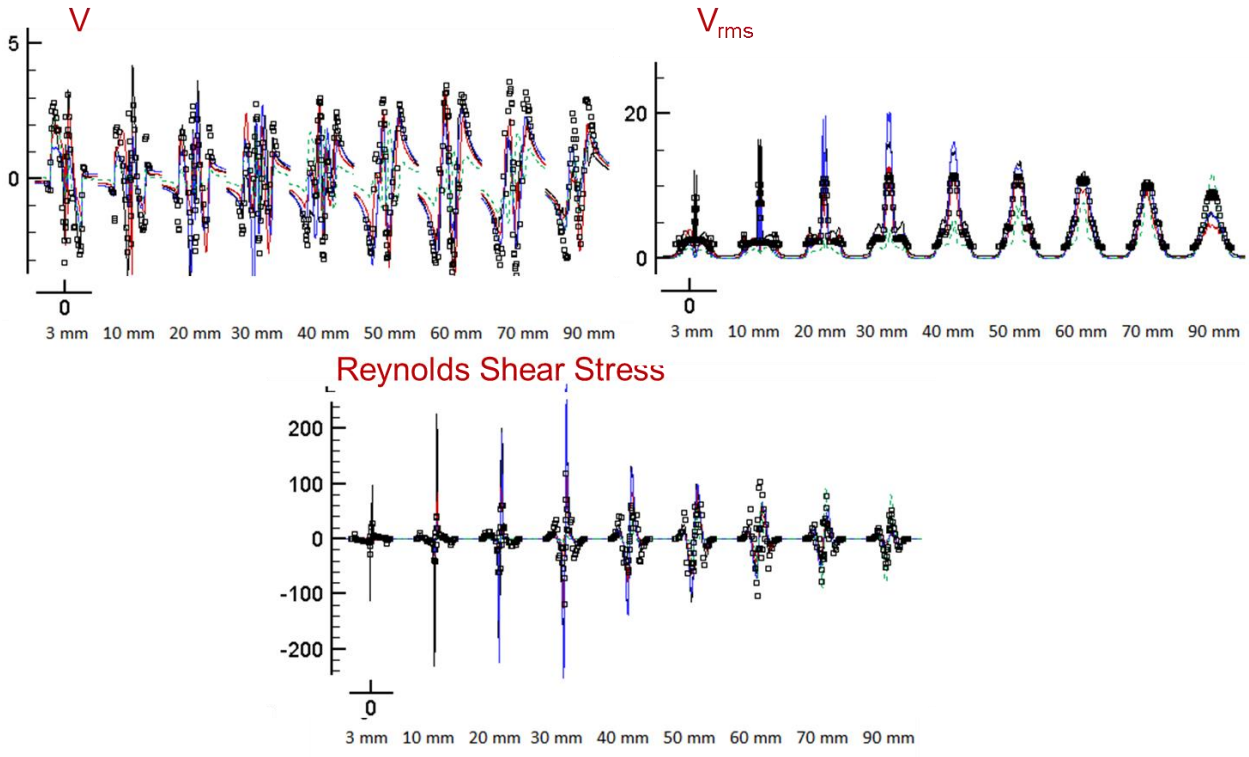

Figure 6: Comparisons with radial mean velocity, radial rms velocity, and Reynolds shear stress

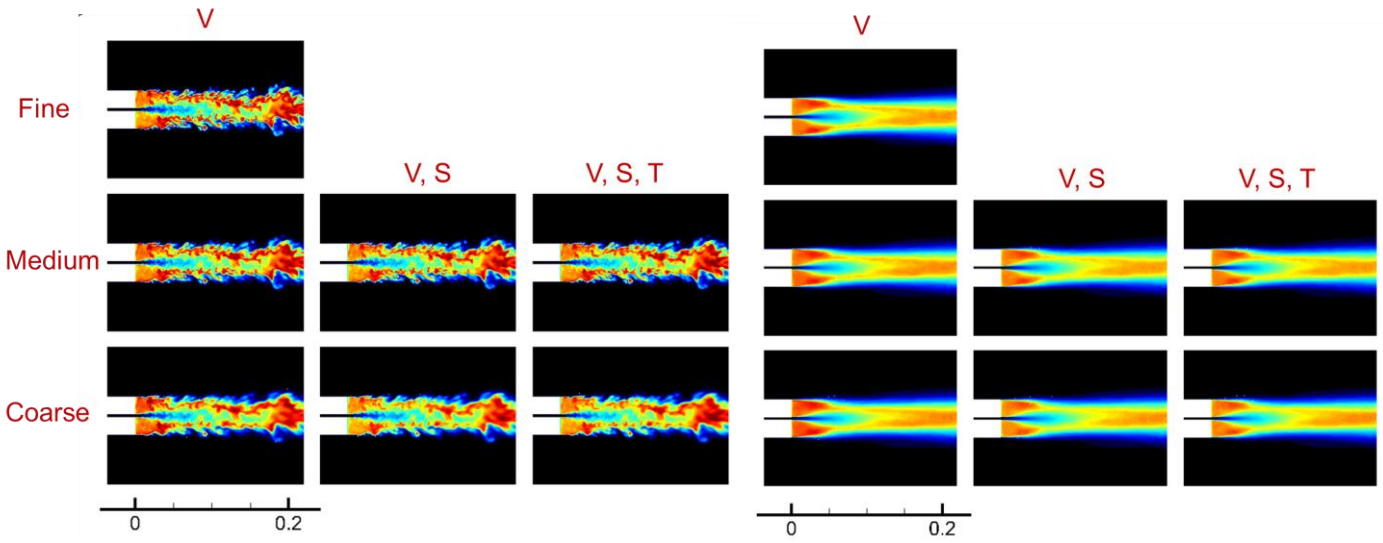

Figure 7. Instantaneous (left) and average (right) centerplane temperature contours for different mesh levels and with different constraints applied.

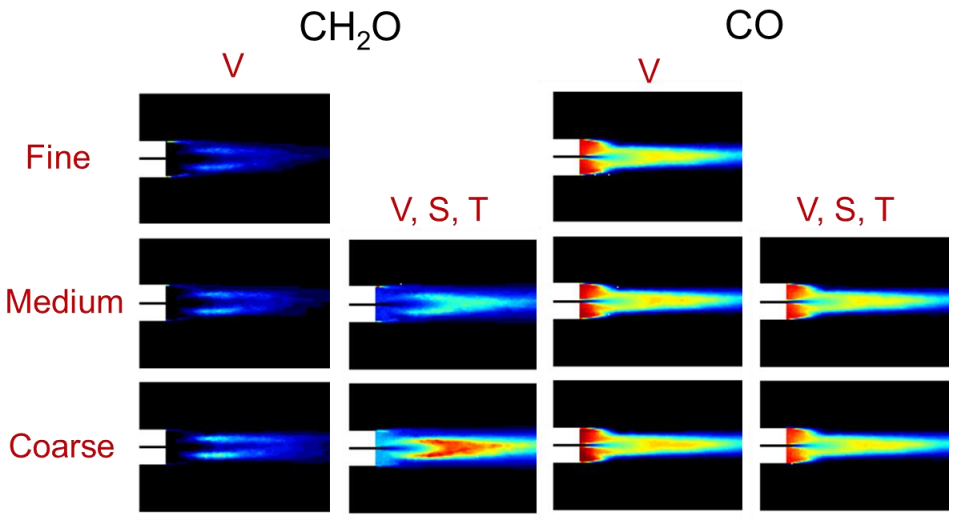

Figure 8: CH_2O and CO mass fraction contours for different mesh levels and with different constraints applied.

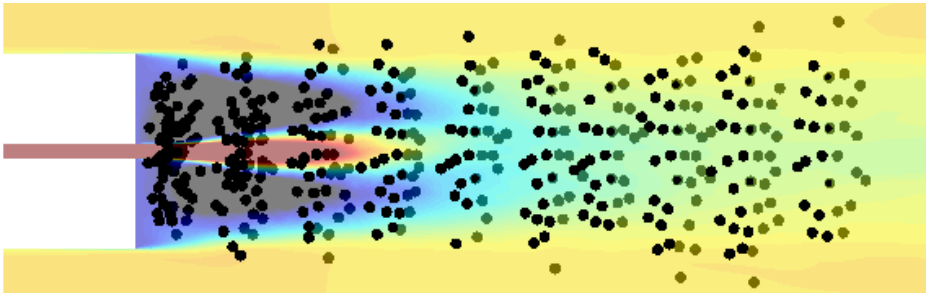

Figure 9. Coarse-mesh data locations used in MRA-MSR.

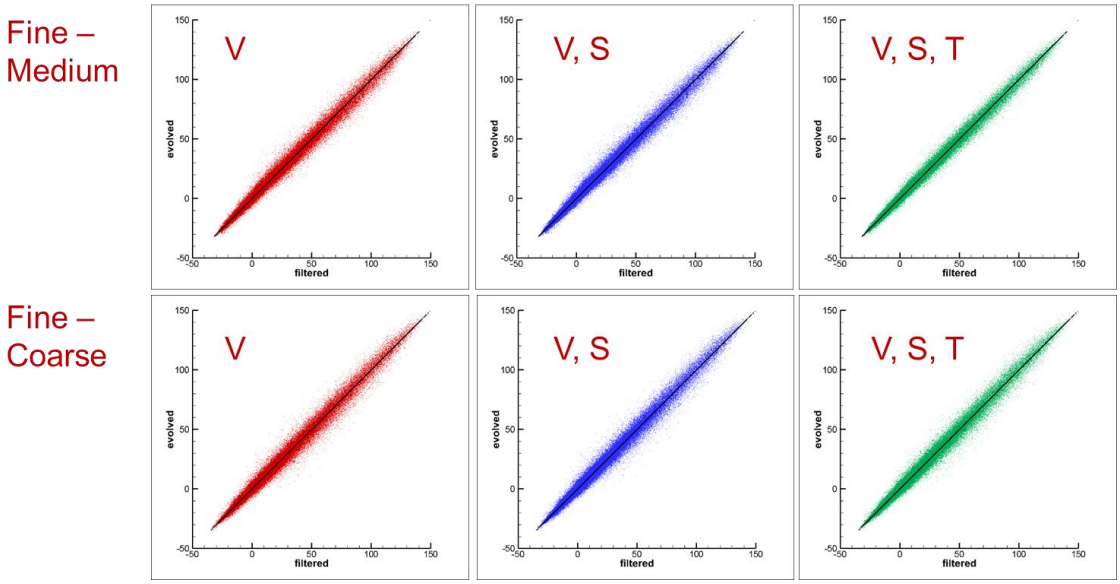

Figure 10. Scatterplot correlations: axial velocity

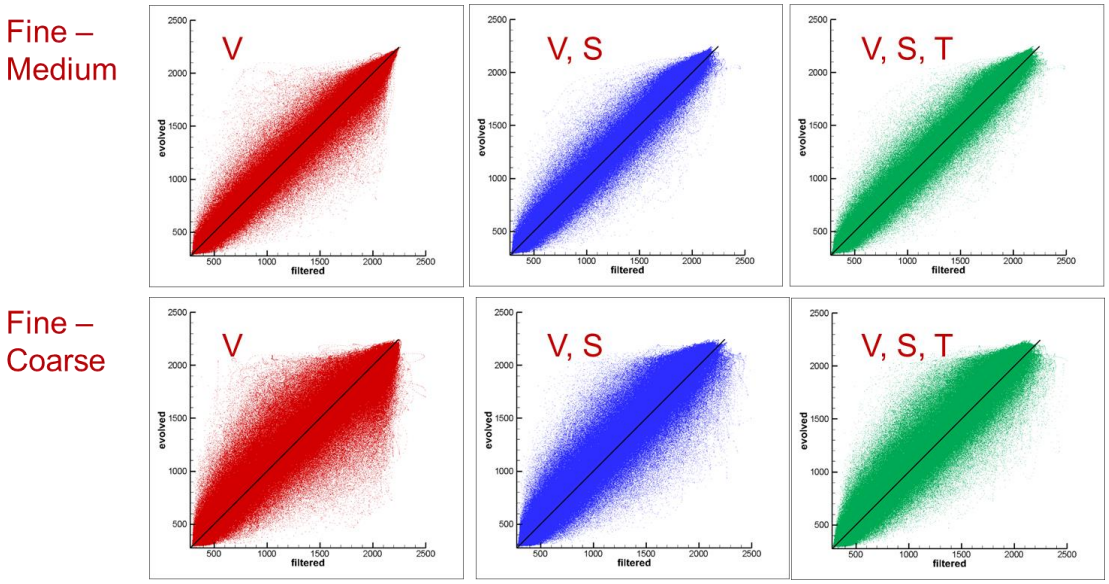

Figure 11: Scatterplot correlations: temperature

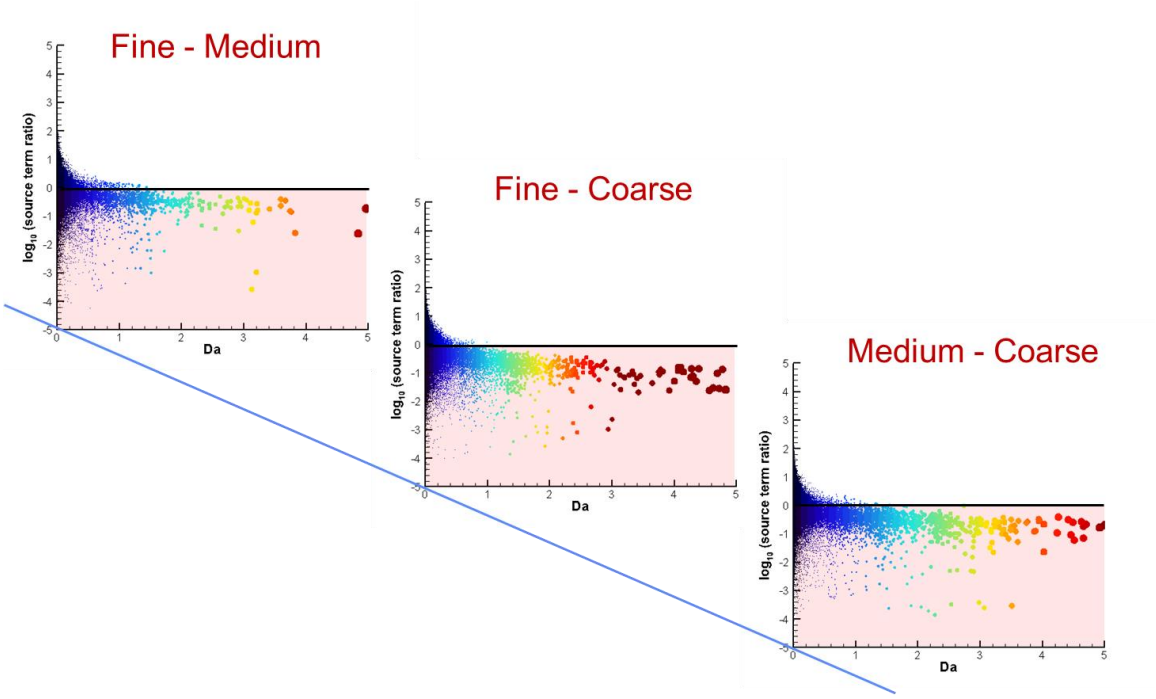

Figure 12: Scatterplot correlations: reactivity measure (ratio of production-rate norms)

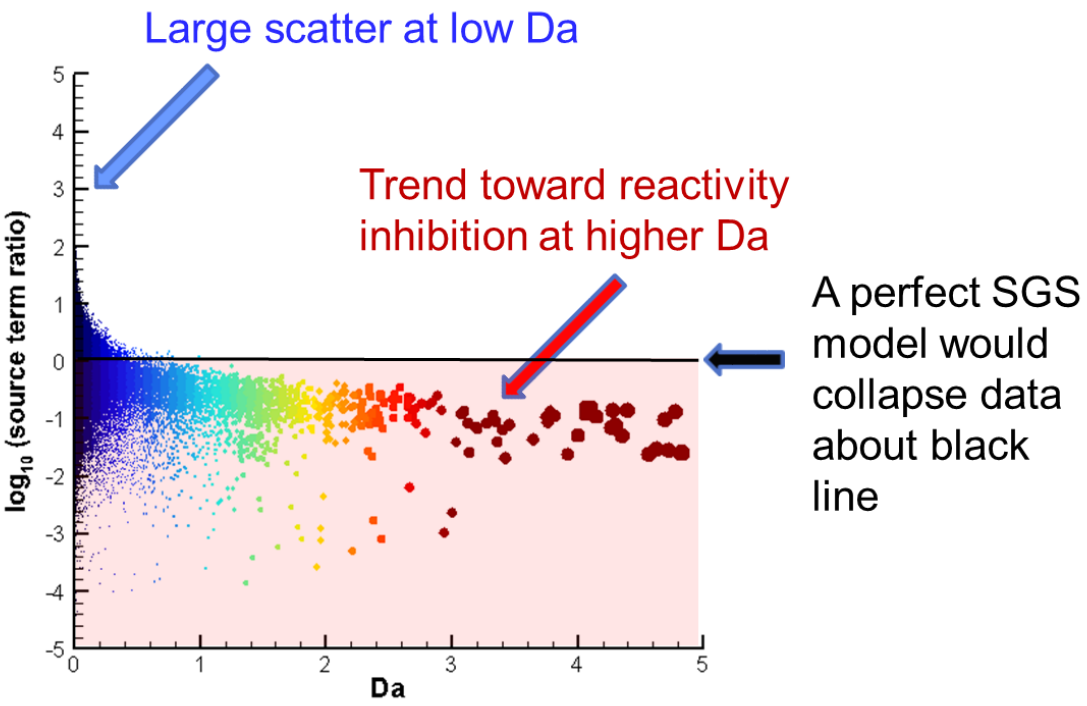

Figure 13: Scatterplot correlation: reactivity measure (explanatory view)

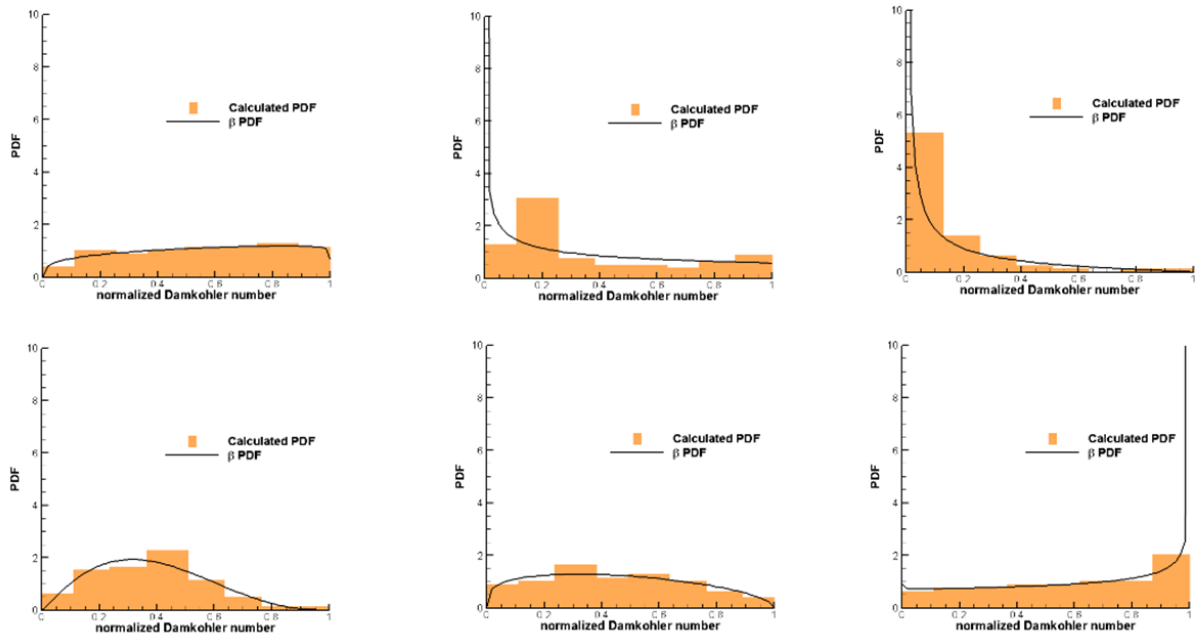

Figure 14: FDFs of normalized Damköhler number extracted from fine-mesh data at different points in space and time

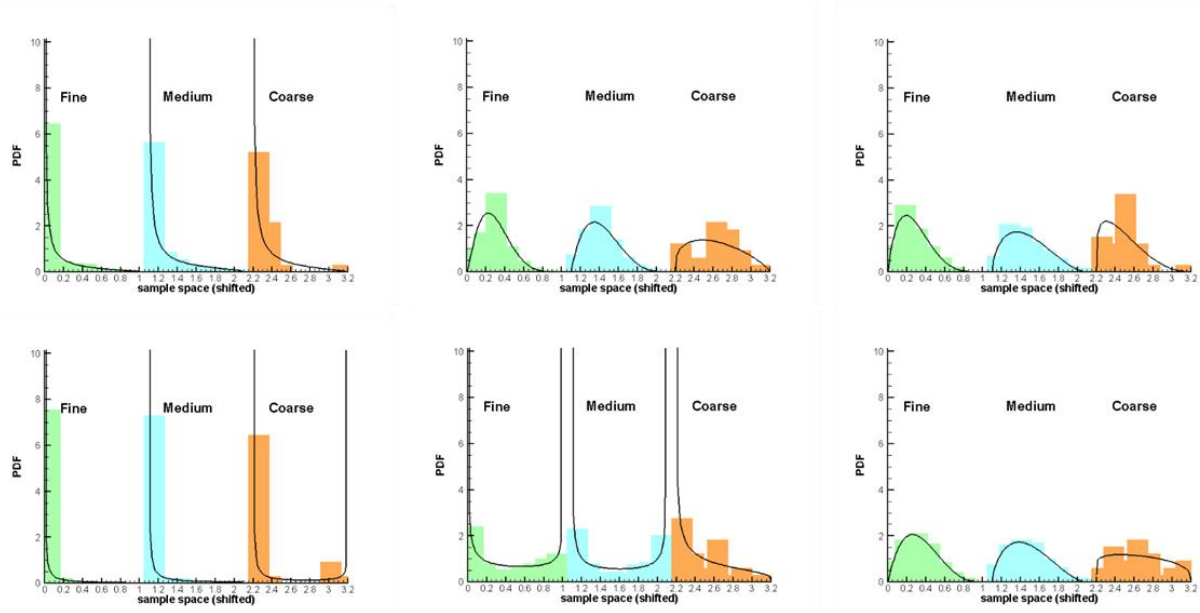

Figure 15: FDFs of normalized Damköhler number at different mesh resolution levels.

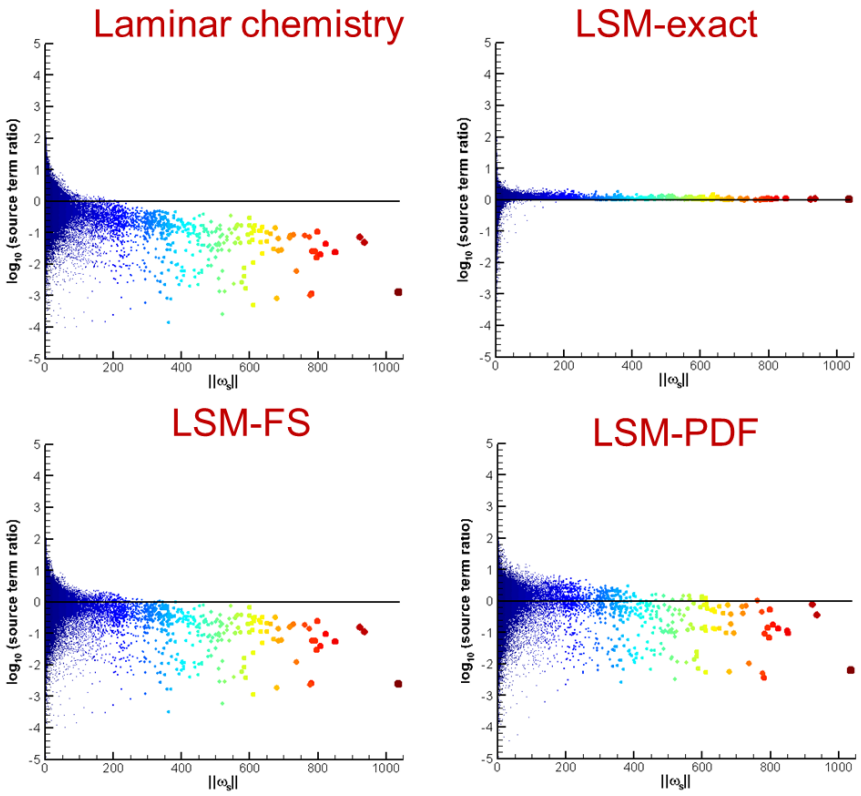

Figure 16: Scatterplot correlations of reactivity measures for different LSM variants (fine-to-coarse interactions)

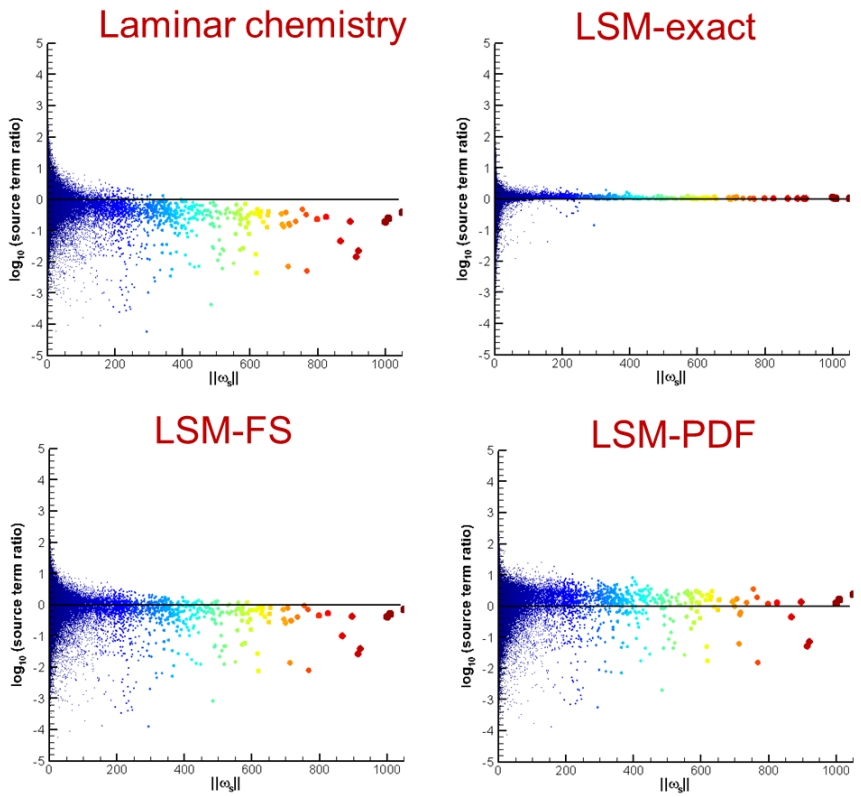

Figure 17: Scatterplot correlations of reactivitymeasures for different LSM variants (fine-to-medium interactions)